Accepted Manuscript

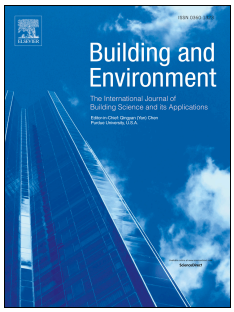

U-value time series analyses: Evaluating the feasibility of in-situ short-lasting IRT tests for heavy multi-leaf walls

Blanca Tejedor, Miquel Casals, Marcel Macarulla, Alberto Giretti

PII: S0360-1323(19)30311-7

DOI: https://doi.org/10.1016/j.buildenv.2019.05.001

Reference: BAE 6123

To appear in: *Building and Environment*

Received Date: 17 February 2019

Revised Date: 2 April 2019

Accepted Date: 1 May 2019

Please cite this article as: Tejedor B, Casals M, Macarulla M, Giretti A, U-value time series analyses: Evaluating the feasibility of in-situ short-lasting IRT tests for heavy multi-leaf walls, *Building and Environment* (2019), doi: https://doi.org/10.1016/j.buildenv.2019.05.001.

U-value time series analyses: Evaluating the feasibility of in-situ short-lasting IRT tests for heavy multi-leaf walls

Blanca Tejedor [a*], Miquel Casals [a], Marcel Macarulla[a], Alberto Giretti[b]

[a] Universitat Politècnica de Catalunya.Department of Project and Construction Engineering. Group of Construction Research and Innovation (GRIC). C/ Colom, 11, Ed. TR5, 08222 Terrassa (Barcelona), Spain

[b] Univeristà Politecnica delle Marche. Department Civil, Building Engineering and Architecture. Via delle Brecce Bianche, 60100 Ancona, Italy

[*]Corresponding author: Blanca Tejedor. Tel: (+34) 93 7398919, E-mail: blanca.tejedor@upc.edu

Abstract

A gap in standardization of quantitative infrared thermography (IRT) directly leads to a lack of measurement pattern for determining in-situ U-values of heavy multi-leaf walls. Three groups of causal factors might influence the estimation of this build quality indicator: operating conditions, thermophysical properties and technical conditions. Focusing on the last one, previous studies underlined the difficulties of measuring below 3 h. In contrast to active IRT, no algorithms have been found to process images, despite playing an important role in the effectiveness and robustness of IRT. The traditional approach involves analysing from 120 to 7200 thermograms with a data acquisition interval of 1 minute up to 1 second respectively. The aim of this paper was to critically assess the test duration that is traditionally used. Six real heavy multi-leaf walls were tested under a stationary regime as a stochastic process of underlying data. For the first time, a research based on two U-value time series analyses (statistical tests and a signal modelling technique by MATLAB) demonstrated the feasibility of short-lasting IRT tests. Moreover, this research posed an innovative data management tool to automate this non-destructive testing (NDT) in mid-term, stopping IRT tests in real time once the right level of accuracy was achieved.

Keywords: quantitative infrared thermography (IRT), in-situ U-value, test duration, time-series analysis, white noise, signal modelling

1. INTRODUCTION

In the last few decades, some researchers have focused on the development and implementation of techniques for assessing building thermal features. Techniques include: simulation [1– 4], the guarded hot box method [5, 6], the automatic guarded hot plate apparatus [7], the heat flux meter method (HFM) [8–15] and infrared thermography (qualitative and quantitative IRT) [16– 28]. In fact, a combination of some of these techniques has been used to complete studies on the influence of boundary conditions on measured U-values [29-34] and to validate results of non-destructive testing (NDT) methods that are not fully developed (i.e. quantitative IRT) [35– 41].

Most of the aforementioned methods have regulations or guidelines on the main requirements and procedures (i.e. guarded hot box: ASTM C177-13 [42], ASTM C1363-11 [43] and UNE-EN ISO 8990:1997 [44]; heat flux meter: ISO 9869:2014 [45]; qualitative IRT: ISO 18434-1:2008 [46], EN 13187:1998 [47] and RESNET Interim Guideline for Thermographic Inspections of Buildings [48]). Recently, ISO 9869-2:2018 [49] has come into force for determining thermal properties (R-value or U-value) of walls with light heat capacity (< 30 $kJ/m^2 \cdot K$) using quantitative IRT under stationary regime. According to this standard, the inner wall surface temperature of a frame structure dwelling is measured using an IR camera, while inner air temperature and the total heat transfer coefficient (assuming convection and radiation processes) are determined by sensors. However, there is a gap in the standardization of quantitative IRT for in-situ building diagnostics of heavy multi-leaf walls that still needs to be filled. This gap causes a lack of measurement pattern, which can affect how the method is applied by practitioners, such as energy auditors or other stakeholders in the construction industry field. Implementation of quantitative IRT encompasses aspects relating to operating conditions (outdoor air temperature), thermophysical properties (the kappa value, also called the heat capacity per unit of area) and technical conditions (test duration and data acquisition interval) [50, 51, 52, 36, 39, 29, 25, 53, 34, 54, 55]. In previous studies conducted in laboratories or experimental rooms, the first two aspects might be considered a source of discrepancy in the determination of the measured U-value, regardless of the technique that has been undertaken (simulation, climatic chamber or HFM) [29, 31, 33, 55]. In real built environments, the influence of operating conditions and non-transient thermophysical properties of the wall was recently analysed with respect to the accuracy of quantitative internal IRT for $\Delta T<10^{o}C$ [56]. This temperature difference was considered a limitation for the method [57, 55].

Focusing on technical conditions, some researchers underlined the difficulties in using quantitative IRT tests with a short sampling duration [58, 37, 38, 39, 59, 55, 60, 61]. Kisilewicz et al. [37] stated that data recorded by an IR camera should be collected for a sufficiently long period (an integer multiple of 24 hours) to determine the thermal resistance reliably and, avoid the fluctuations in temperature and heat flows. Carbonez et al. [59] considered that instantaneous IRT measurements only provided a single value in time and consequently, both the applicability and accuracy of the method were limited. Lucchi [55] pointed out that U-values obtained by IRT were often found to be a bit lower than those resulting from HFM. Each wall composition may need to be tested by specific NDT. Otherwise, a long-lasting test should be executed to provide more reliable results [55]. Generally, the usual approach for analysing IRT readings assumes that longer test duration leads to greater accuracy in the quantitative IRT method.

However, a thorough literature review has shown the use of different test durations and data acquisition intervals, which might also lead to a discrepancy in the assessment of in-situ U-values. The minimum test duration for the quantitative IRT method has been set at 2–3 hours under stationary conditions [36, 38, 62, 63, 54]. Regarding sampling frequency, a random criterion was detected for HFM and quantitative IRT [64]. Fokaides et al. [38] measured the surface temperature every 20 minutes for 3 hours and the U-value was the result of the average of the 10 measurements for each building element. Marinetti et al. [65] took 30 thermograms with a sampling interval of 10 seconds. Dall'O et al. [39] established a data acquisition interval of about 15 minutes, but only some sub-periods were suitable for the measurement. Lehmann et al. [29] selected a sequence of single thermograms taken at 5-minute intervals. Porras – Amores et al. [66] recorded images every 10 seconds and temperature readings every 1 second. De Freitas et al. [40] carried out 6 thermograms for each sunny day at different sampling intervals (3 h, 4 h, 1 h, 1 h and 5 h). Fox et al. [27] captured images every 20 to 30 minutes. Tejedor et al. [54] and Tejedor et al. [56] configured all the measuring equipment with a data acquisition interval of 1 minute, recording from 120 to 180 thermograms as the maximum. Bienvenido –Huertas et al. [64] proposed a sampling period of 15 minutes to facilitate the subsequent data analysis. Taking into account the aforementioned sampling durations and sampling frequencies, the usual approach adopted for this NDT could imply to manually post-process from 120 to 7200 thermograms with data acquisition intervals of 1 minute to 1 second respectively.

The number of thermograms has a direct impact on test execution. During the monitoring procedure, a sequential video is recorded. Such video is comprised of a number of frames or thermograms corresponding to the sampling frequency. In the processing stage, the instantaneous reading of the reflected ambient temperature (T_{REF}) must be read and updated in the software by the technician, to obtain a reliable instantaneous reading of the wall surface temperature (T_{WALL}) for each thermogram (Figure 1a). Otherwise, the IR camera software takes the T_{REF} that was measured at the beginning of the test by default for all images gathered during 2 to 3 hours of test duration, leading to no compensation of the errors for each instantaneous reading provided by the IR camera (Figure 1b). This is a significant issue, since the reflected ambient temperature might change throughout the IRT survey as the inner air temperature (T_{IN}) increases in the same way that the reflection indexes of objects around the target may change.

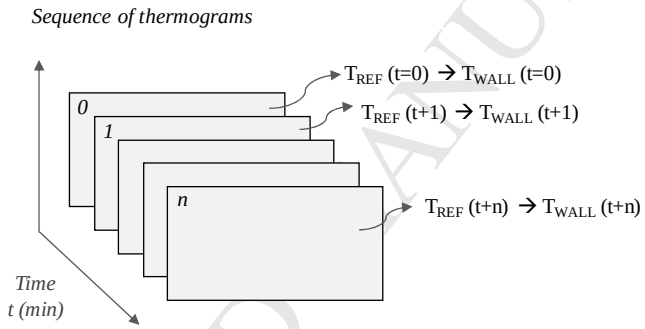

(a) Manual processing stage of IRT measurements by the technician

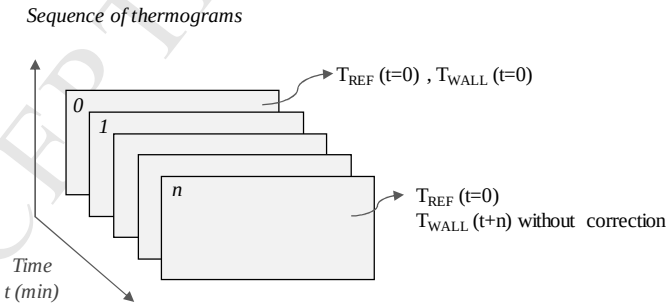

(b) Processing stage of IRT measurements that software executes by default

Figure 1. Description of the analysis of thermograms for the quantitative IRT method

To resolve this lack of robustness of the method and avoid the human factor as an added source of discrepancy, an algorithm should be required during the thermographic survey. Nevertheless, a literature review did not reveal approaches to quantitative internal IRT in which the readings of in-situ tests in building envelopes were automated under a stationary regime. Algorithms have been developed to

process images under transient conditions for manufacturing processes and applying active IRT [67–72]. Montanini et al. [70] and D'Accardi et al. [72] enhanced the readability of images through a comparative analysis of data processing algorithms for detecting defects with active IRT: Pulsed Phase Thermography (PPT), Slope, Thermographic Signal Reconstruction (TSR), Guided Filtering (GF), Logarithmic Transformation (LN), Principal Component Analysis (PCT) and Correlation Coefficient (R^2). The R^2 was executed by IRTA Software [73], while the rest of the approaches were implemented using the MATLAB "Programming Environmental Toolbox" [74]. Mathematical processing methods play an important role in the effectiveness of IRT [71], since the assessment of IR maps takes a considerable amount of time [72]. In fact, future optimization of the processing parameters (i.e. number of evaluated frames) will be required to achieve better results in a minor time [72]. For this reason, quantitative IRT proposals should take into account the above aspects and probably work with signal modelling techniques.

In this context, the aim of the research was to critically evaluate the role of test duration and the feasibility of conducting short-lasting IRT tests in the determination of in-situ thermal transmittances of heavy multi-leaf walls from inside the building. Firstly, the measurements of six real façades under steady-state conditions were assessed to estimate the average U-value for several sampling durations. In this way, it was possible to check the assumption adopted by previous researchers, in which the NDT must be performed with long sampling durations to ensure higher accuracy. Secondly, monitored data were statistically evaluated as a stochastic process. In other words, quantitative IRT measurements were assumed as a U-value time series constituted by a constant signal plus random error. Subsequently, a second U-value time series analysis was computed through a signal modelling technique based on the MATLAB "System Identification Toolbox" [75]. Finally, considering the results of both studies, a routine for processing and stopping IRT tests is proposed. It should be noted that all case studies fall outside the scope of ISO 9869-2:2018 [49]. In addition, standardized methods (i.e. HFM) were not executed. Nardi et al. [76] and O'Grady et al. [77] stated that heavy walls show a low discrepancy (1.3 – 2.6%) between the measured U-values determined by HFM and IRT, in contrast to light walls (>47.6%).

The paper is structured as follows. Section 2 describes the research methodology used in this paper and the investigated building façades. Section 3 discusses the results and Section 4 exposes the main conclusions of this research.

2. METHODOLOGY

The research methodology was structured in three steps that are fully described in Sections 2.1. (The role of test duration on the accuracy of quantitative internal IRT measurements), 2.2. (U-value time series analysis using statistical tests) and 2.3. (U-value time series analysis by signal modelling technique).

2.1. The role of test duration on the accuracy of quantitative internal IRT measurements

As mentioned in the literature review, previous researches highlighted the use of a short test duration as a significant limitation of the quantitative IRT method. However, a random criterion for conducting the tests was detected. For this reason, the first part of this study was focused on analysing whether the deviation between theoretical and measured U-value ($\Delta U/U_t$) decreased as sampling duration was longer, following the usual approach for quantitative thermography in which the input data of the numerical model is manually processed. The measurement campaigns were conducted on six typical Spanish heavy multi-leaf walls from January to March 2017, to ensure a correct implementation of this NDT in accordance with Tejedor et al. [54] (specifications of the developed method) and Tejedor et al. [56] (recommendations about influential operating conditions). The details of each investigated building envelope are given below, with information drawn from the construction documents (Figure 2; Table 1).

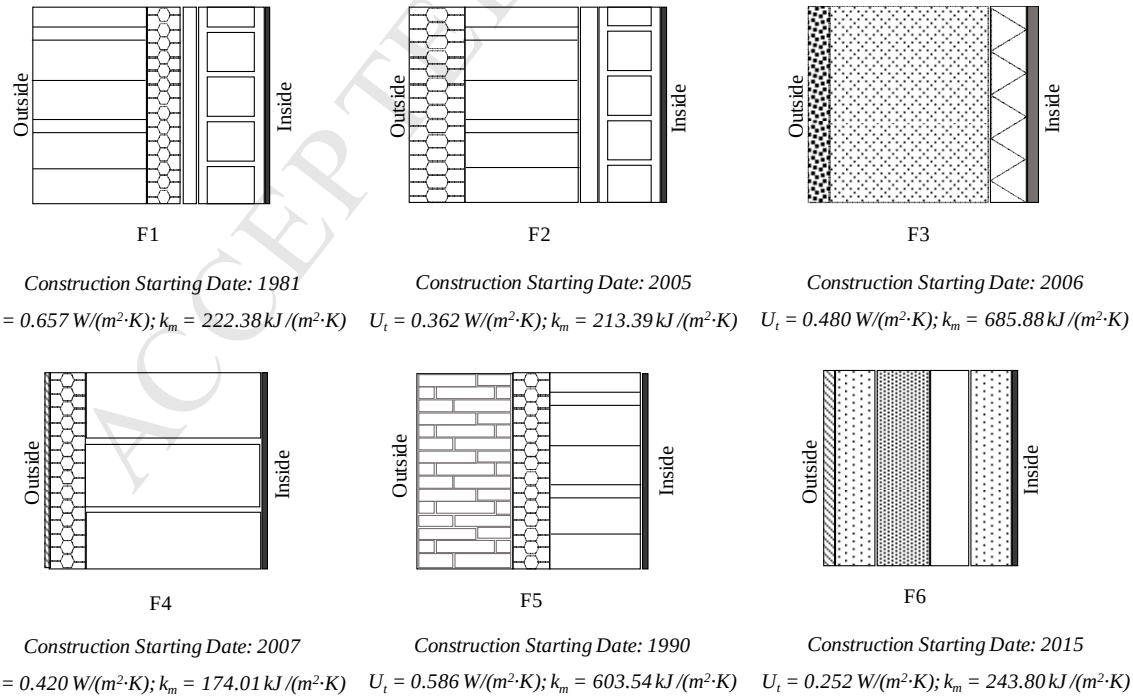

Figure 2. Schematic sections of the building envelopes and their construction starting date

159 Table 1. Configuration and technical features of the façades (from outside to inside)

	N#	Material layer	Δx_i [m]	λ_i [W/(m·K)]	ρ_i [kg/m^3]	$c_{p\,i}$ [J/(kg·K)]	$R_{t\,i}$ [(m^2·K)/W]	L [m]
F1	1	Perforated brick wall	0.140	---	1140	1000	0.180	2.50
	2	Insulation EPS	0.030	0.033	30	1400	0.909	
	3	Non-ventilated air cavity	0.020	---	1	1004	0.160	
	4	Hollow brick wall	0.050	---	1000	1000	0.070	
	5	Gypsum plaster	0.010	0.300	1150	1000	0.033	
F2	1	Insulation EPS	0.080	0.038	20	1400	2.125	2.70
	2	Perforated brick wall	0.140	---	1140	1000	0.180	
	3	Non-ventilated air cavity	0.050	---	1	1004	0.180	
	4	Hollow brick wall	0.040	---	1000	1000	0.090	
	5	Gypsum plaster	0.010	0.570	1150	1000	0.018	
F3	1	Limestone wall	0.030	2.300	2395	920	0.013	2.51
	2	Reinforced concrete wall	0.250	2.300	2400	1000	0.109	
	3	Rock wool insulation	0.064	0.037	40	840	1.730	
	4	Plasterboard	0.016	0.250	825	1000	0.064	
F4	1	Mortar	0.002	1.300	1900	1000	0.002	2.54
	2	Insulation EPS	0.060	---	20	1400	1.620	
	3	Thermoclay	0.240	---	910	719	0.570	
	4	Gypsum plaster	0.010	0.570	1150	100	0.018	
F5	1	Stone wall	0.180	2.200	2300	1000	---	2.45
	2	Insulation EPS	0.040	0.040	24	1340	---	
	3	Perforated brick wall	0.150	0.350	1140	1000	0.180	
	4	Gypsum plaster	0.015	0.570	1150	1000	0.018	
F6	1	Mortar	0.015	0.550	---	---	---	2.64
	2	Lightweight concrete	0.060	0.125	---	---	---	
	3	PIR insulation	0.080	0.028	---	---	---	
	4	Non-ventilated air cavity	0.060	---	---	---	0.180	
	5	Lightweight concrete	0.070	0.125	---	---	---	
	6	Gypsum plaster	0.015	0.430	---	---	---	

160 *Δx_i : thickness of the layer; λ_i: thermal conductivity of the layer; ρ_i: density of the layer; $c_{p\,i}$: specific heat capacity of the layer; $R_{t\,i}$:*

161 *notional thermal resistance of the layer; L: height of the wall*

162

163

As shown in Figure 2, all the samples were from different construction periods. Façades F1, F2 and F5 were erected under the first thermal regulation that came into force (NBE-CT-79 [78]). The rest of the building envelopes were built under the current Spanish Technical Building Code (CTE-DB-HE1 [79]). The main technical features of each wall layer were taken from construction project documents and manufacturers' datasheets (Table 1). To determine the theoretical U-value, UNE-EN ISO 6946:2012 [80] and the Spanish Technical Building Code CTE-DB-HE1 [79] were applied. Finally, UNE-EN ISO 13786:2011 [81] and UNE-EN ISO 10456:2012 [82] were undertaken to calculate the heat capacity per unit of area.

Concerning the calculation procedure, few researchers have used quantitative internal IRT in their studies to determine the measured U-value [38, 33, 54, 56]. For its implementation in a real built environment, it can be considered that the building envelope is crossed by one-dimensional horizontal specific heat flux (q) resulting from convection (q_c) and radiation (q_r) processes, without the impact of any sort of external thermal stimulus (i.e direct solar radiation) and under quasi steady-state conditions. According to the method proposed by the authors [54], the instantaneous measured thermal transmittance [W/m^2·K] is expressed by Equation 1:

$$U_{mes_i} = \frac{\left\{0.825+\frac{0.387\cdot R_a^{\frac{1}{6}}}{\left[1+\left(\frac{0.492}{Pr}\right)^{\frac{9}{16}}\right]^{\frac{8}{27}}}\right\}^2 \cdot \lambda_{air}}{L} \cdot [T_{IN}-T_{WALL}]+\varepsilon_{WALL}\cdot\sigma\cdot[{T_{REF}}^4-{T_{WALL}}^4] \over (T_{IN}-T_{OUT})} \quad (1)$$

Where ΔT is the air temperature difference between inside and outside the building in [K], which involves the inner and outer air temperatures (T_{IN} and T_{OUT} respectively) in [K]. Other parameters in the equation are: wall surface temperature (T_{WALL}) in [K]; reflected ambient temperature (T_{REF}) in [K]; wall surface emissivity (ε_{WALL}) with a value of 0.88 for gypsum plaster; Stefan–Boltzmann's constant (σ) with a value of 5.67x10^{-8} [W/m^2 ·K^4]; air thermal conductivity (λ_{air}) measured in [W/m·K]; wall height (L) seen from inside the building in [m]; and dimensionless parameters Rayleigh (R_a) and Prandtl (P_r) numbers for a laminar flow.

To measure and record the environmental parameters (T_{IN} and T_{OUT}), two data loggers with type K thermocouples (TF-500, PCE –T390, PCE Iberica SL) were used. Their resolution and accuracy were set at 0.1ºC and ± 0.4% +0.5ºC. To monitor the parameters related to the building envelope (ε_{WALL}, T_{REF} and T_{WALL}), the following elements were installed: a reflector (crinkled aluminium foil as a substitute for Lambert's radiator with dimensions 0.20 x 0.15 m); a blackbody (taking as a reference a black tape with emissivity equal to 0.95 and dimensions 0.01 x 0.05 m); and an IR camera of long wavelength band (7-13 μm of the spectral range). The thermal camera (FLIR60bx, FLIR SYSTEMS) had a field of view of 25x19º, an IR resolution of 320 x 240 pixels (thermal sensitivity <0.045ºC at 30ºC) and an accuracy of ± 2ºC or 2% reading at ambient temperature (10 to 35ºC). Each thermogram was post-processed using the sequential video of 120 minutes provided by FLIR TOOLS + software [83].

Once instantaneous measured U-values had been calculated, the mean ($U_{mes\ avg}$) was estimated from the total number of thermograms (n) [Equation 2]:

$$U_{mes_{avg}} = \frac{\sum_{i=1}^{n}(q_{c_i}+q_{r_i})}{\sum_{i=1}^{n}(T_{IN_i}-T_{OUT_i})} = \frac{\sum_{i=1}^{n} U_{mes_i}}{n} \quad (2)$$

2.2. U-value time series analysis using statistical tests

Theoretically, the instantaneous measured U-values ($U_{mes\ i}$) should define a constant mean over time that would be known as $U_{mes\ avg}$ or $\bar{U}$ [W/ (m^2· K)] and would be obtained at the end of an IRT survey from a specific number of thermograms (n), as shown in Equation 2 of Section 2.1.

Nevertheless, it can be assumed that the quantitative internal IRT measurements describe a stochastic process of underlying data in practice, since a time series is a set of consecutive samples collected over a time interval and they are ubiquitous in any field that involves data monitoring [84, 85]. Moreover, time series can lead to an understanding of evolving processes or provide information about trends [85].

Figure 3 is shown to support the above assumption. The instantaneous measured U-values draw a constant signal as a function of time with a certain noise [e_k *(t)*] that is characterized by random values with a constant mean and variance, normally and independently distributed, and uncorrelated (Equation 3). In accordance with Mahan et al. [85], this last aspect is known as "white noise".

$$U(t) = \bar{U} + e_k(t) \quad (3)$$

Hence, the hypothesis of a stochastic process comprised of a constant signal plus white noise might be evaluated for a U-value time series with different test durations.

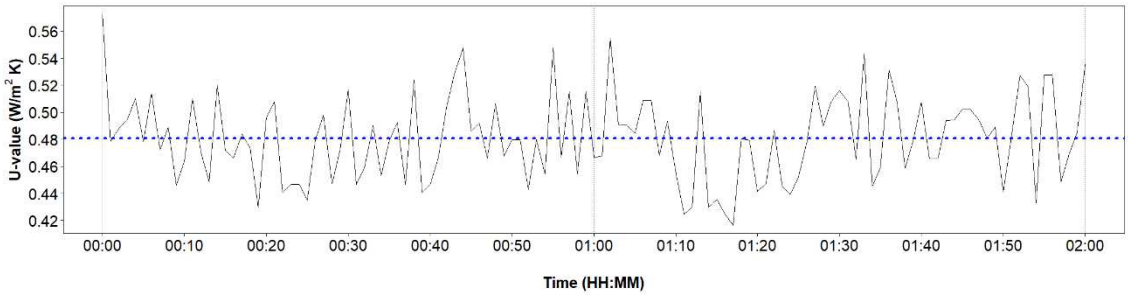

Figure 3. Example of a quantitative internal IRT test taken as a stochastic process

In accordance with the above statement, measurement noise [e_k *(t)*] might also be determined over time, assuming this parameter as the residuals if [*U(t)*] is modelled as a constant signal (Equation 4). To confirm that the measurement noise is fitted to white noise, the autocorrelation function (ACF) and the cumulated periodogram (CP) were used. Both had been used in previous studies in other fields that involved monitored data [86–89].

$$e_k(t) = \bar{U} - U(t) \quad (4)$$

The ACF measures the correlation between observations at different times [90]. When a process is non-stationary, it does not tail away to zero quickly or cut-off after a finite number of steps [85]. Hence, the ACF of the signal should not contain more statistically significant terms than the number expected by chance. This depends on the number of lags or delays [85], which is one time unit for the first-order autocorrelation [90].

The CP is the vector of partial sums of the periodogram, normalized by the sum of all elements. Since the Fourier transform of the residuals is obtained by a linear transformation with an orthogonal matrix, the real and imaginary parts of the transform model would still be distributed independently and normally [91]. The test is focused on constructing two lines parallel to the one above and passing through the ±5%

point of the Kolmogorov-Smirnov statistics. These lines define a 95% confidence interval for white noise [92, 91].

In both statistical tests, the analysis was computed for 120, 60 and 30 minutes of test duration. These data points coincide with the number of thermograms that were post-processed, since the data acquisition interval was 1 minute. The limitation related to minimum data points was supported as follows. Roughly speaking, a sample size of at least 40–100 repeat observations was recommended. Otherwise, due to sampling error, the estimated functions might not contain enough information for a meaningful identification [93–97]. However, statisticians and researchers adopted a general criterion based on the central limit theorem (CLT) in which the sample size should be $N \geq 30$ in practice, to assume the distribution of sample mean approximated to the normal distribution [98, 99]. The shapes of probability distributions may vary for $N \leq 30$ [99].

Finally, to determine the variability among the instantaneous U-values of each time series for all investigated buildings, the following parameters were calculated: the mean ($\bar{U}$), the standard deviation (SD or σ), and the coefficient of variation (CV). Subsequently, the 95% confidence intervals were also statistically estimated to observe whether the readings of each time series were equal. In other words, the aim was to evaluate whether there was a relevant difference among average measured U-values resulting from 120, 60 and 30 minutes. The following expression (Equation 5) was applied to calculate the 95% confidence intervals (CI), considering that *n* is the specific number of thermograms or data points to be analysed:

$$CI(95\%) = \bar{U} \pm 1.96 \cdot \frac{\sigma}{\sqrt{n}} \quad (5)$$

2.3. U-value time series analysis by signal modelling technique

Wiener [100] and Brown et al. [101] carried out several studies about extrapolation, interpolation or smoothing of stationary and transient time series for engineering applications. Later, some authors compared inverse heat conduction problems (IHCP) using experimental data to determine thermal properties of materials [102–106]. Le Niliot et al. [104] combined thermographic measurements with numerical techniques to identify unknown heat line sources and boundary conditions for the transient

diffusion problem. Ilyinsky et al. [103] and Rainieri et al. [105] determined the local distribution of the heat transfer coefficient in thermal systems by applying a filtering technique to remove the undesired noise assumed as random uncertainties in temperature measurements. Their methods were based on the Fourier Transform technique to estimate the heat source distribution in a square domain, taking the surface map recorded by an IR camera as a starting point. Rainieri et al. [105] applied this type of analysis to compact heat exchangers. They concluded that the Wiener filter might be more efficient than other traditional filtering procedures, using the MATLAB "Signal Processing Toolbox" and "Image Processing Toolbox" [107, 108]. Jiménez et al. [109] applied the MATLAB "IDENT Toolbox" [110] to calculate the thermal properties of building elements for tests undertaken from outside the building under transient conditions. In that study, they stated that the RC-network can be formulated as ARMAX or ARX models by means of MATLAB. In addition, only ARX models could simplify the analysis without loss of generality. If the predictions were correctly calculated, then the one-step prediction error or residual could be considered as white noise sequence [109]. Notably, the ARX (autoregressive model with external input) is known as one of the simplest parametric structures, while the ARMAX (autoregressive moving average model with external input) is interesting and useful when dominating disturbances appear early in the process [111].

To support the results obtained in the first U-value time series analysis (Section 2.2), an alternative recognized method must be applied. Taking into account the aspects mentioned above, the MATLAB "System Identification Toolbox" [75] was chosen for this study. Firstly, operation pre-processes of the signal (i.e. filters) and several models (such as ARX and ARMAX) were developed, with the IRT data introduced into the MATLAB "System Identification Toolbox" [75]. Secondly, to detect whether the results provided by reduced order models were correct, the following aspects were checked: the stability of the model, the resonance state in the frequency response plot, the distribution of zeros and poles, the ACF of the residuals at 95% confidence level. Thirdly, the modelled signals, the instantaneous measured U-values and the theoretical U-values were plotted against time for each building envelope. In this way, MATLAB allowed observing whether the system was under steady-state conditions for sampling durations < 120 minutes and if the hypothesis adopted in Section 2.2. was also fulfilled.

3. DISCUSSION OF RESULTS

3.1. The role of test duration on the accuracy of quantitative internal IRT measurements

This section pretends to discuss if longer test durations entail significant accuracy differences among data packages. The measured U-values of each wall and their respective deviations with the theoretical thermal transmittance ($\Delta U/U_t$) were determined for 2 hours of sampling duration and a data acquisition interval of 1 minute, following the process extensively reported in Tejedor et al. [54] and refined in Tejedor et al. [56] through the analysis of the most influential operating conditions. Subsequently, the deviations between theoretical and measured U-value were plotted against time (120, 60, 30 and 15 minutes).

As can be observed in Figure 4, the optimum deviations between theoretical and measured U-values (indicated with a red circle) fluctuated over time. The lowest gap was obtained by F3 and F4 after only 30 minutes of the test, since $\Delta U/U_t$ were found to be 0% and 1.19% respectively. F1 and F5 presented a deviation of 0.46% and 3.41% after 60 minutes of the test. The best results for F2 and F6 were gathered at 120 minutes, with an error of 9.39% and 1.98% respectively. Therefore, it seems that long-lasting tests do not always ensure more accurate outcomes, since only 2 case studies led to obtain lower errors with longer measurements (120'). Consequently, it seems that the usual approach for establishing test duration might not be considered to standardize this NDT.

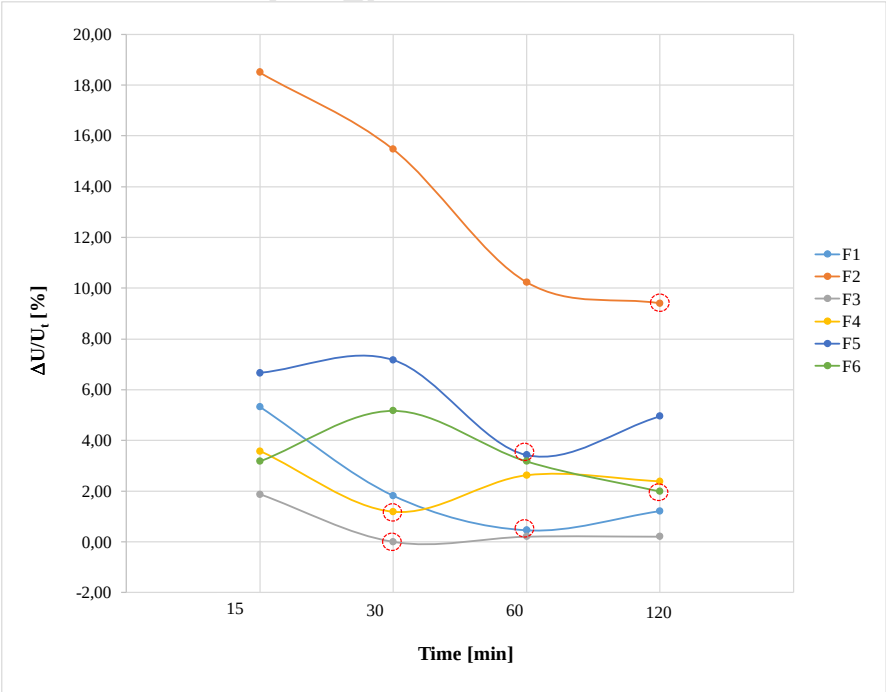

Figure 4. Deviation of the measured U-values over time

Some boundary conditions were given during the execution of this NDT:

- The wind speed was found to be lower than 0.5 m/s for all case studies, avoiding the thermal dispersion of convective factors around the external wall surface. According to Albatici et al. [36] and Dall'O et al. [39], the accuracy of this NDT could be affected by the wind speed, especially in walls with low thermal mass since they cool down faster. Nevertheless, and considering that the current research was performed on heavy multi-leaf walls (k_m > 150 kJ/m^2·K), the impact of wind speed was negligible.
- The measurements were conducted on northern façades in the early morning, avoiding the direct solar radiation. Otherwise, the influence of this external thermal stimulus might not have been easily predictable and consequently, the IRT survey would have been performed on dynamic heat transfer conditions. Neither indoor sides of the buildings were exposed to direct sunlight through adjacent windows.
- In previous studies, Tejedor et al. [54] and Tejedor et al. [56] demonstrated that the optimum schedule was from 6 a.m. to 9 a.m. during the winter. Outside temperatures ranged from 0 to 5º, resulting the period of day with minimum fluctuations.
- Façades F1 to F4 belonged to unoccupied residential buildings that had neither electric nor heating sources. In fact, they had not been occupied for years (F1) or they had not been in-use since their construction stage (F2, F3, F4). These aspects lead to perform quantitative IRT inspections under an inner air temperature of 12-14ºC and within the optimum temperature difference range set by Tejedor et al. [56].
- Façades F5 and F6 presented a heating system in operation. F5 was a residential building that had only been used in certain seasonal periods of the year (summer or winter). The control of the heating system was centralized and the thermographer could not modify the inner temperature set point. For this reason, the test was performed for 18.30 < ΔT < 19.60ºC. F6 was a new building mock-up in real scale based on prefabricated panels with structural and insulation functions as well as incorporated facilities to be configured by the user or thermographer.
- The thermal conductivity of the air (λ_{air}) was assumed to be 0.024 W/m·K for the unoccupied buildings that formed part of public housing stock (F1 to F4) and their electric or heating systems were not switched on (T_{IN} =0-15ºC). For buildings with a heating system in operation (F5 and F6), this parameter was set at 0.025 W/m·K (T_{IN}=15-25ºC) [56].

- Considering laminar flux, the dimensionless parameters Rayleigh (R_a) and Prandtl (P_r) numbers should be determined. The Prandtl (P_r) number was assumed to be 0.73 for T_{IN}=0–25ºC. However, the Rayleigh number (Equation 6) should be calculated in accordance with Tejedor et al. [56], since it mainly depends on the inner air temperature (T_{IN}) and the wall surface temperature (T_{WALL}):

$$R_a = G_r \cdot P_r = \frac{g \cdot \beta \cdot (T_{IN} - T_{WALL}) \cdot L^3}{v^2} \cdot P_r \quad (6)$$

Where G_r is the Grashof number; g refers to gravitation (9.8 m/s^2); β is the volumetric temperature expansion coefficient [1/K] that is defined by $\beta = 1/T_m$, where $T_m = (T_{IN} + T_{WALL})/2$; v is the air viscosity with a value of $1.4 \cdot 10^{-5}$ m^2/s for T_{IN}= 0–15ºCand $1.5 \cdot 10^{-5}$ m^2/s for T_{IN}=15–25ºC.

The formulation and tabulated values of the thermal conductivity of the air, the Prandlt and Rayleigh numbers and the air viscosity were taken from several sources [112–116], including the values provided by EES Software [117].

3.2. U-value time series analysis using statistical tests

Roughly speaking, the first U-value time series analysis reported in Section 2.2. might provide enough statistical information to detect whether the IRT signal draws cycles. This could indicate that the quantitative internal IRT test is being executed under a transitory regime or more observations are required with a data acquisition interval of 1 minute to achieve reliable U-values.

An in-depth analysis of the residuals of the measured data for each building façade as well as their respective ACF and CP is reported in Figures 5–10. At the end of this section, the key features are summarized, and supported by Tables 2–3 and Figure 11. Table 2 shows the main parameters to evaluate the variability among instantaneous U-values ($\bar{U}$, σ, CV). It highlights whether the hypothesis of constant signal plus white noise could be adopted for all heavy walls. Table 3 compares the mean, standard deviation and coefficient of variation between packages of sampling duration (120 vs. 60 minutes; 60 vs. 30 minutes; 120 vs. 30 minutes). In this way, it is possible to quantify the variability degree. Figure 11, which is a graphical representation of 95% confidence interval (CI) for U-value estimations, allows observing if the measurement errors could be accepted or tolerated in order to reduce the test duration.

Façade F1 was characterized by an average thermal transmittance of 0.665 W/m^2·K for 120 minutes, 0.654 W/m^2·K for 60 minutes and 0.645 W/m^2·K for 30 minutes (Table 2). The left graphs of Figure 5 plot the noise [e_k *(t)*] of in-situ measured U-values as a function of time. Discontinuous black lines represent the average value, that is 0, and discontinuous blue lines represent ±σ. The e_k values reached peaks of between 0±0.08 W/m^2·K and 0±0.12 W/m^2·K. From the above aspects, it can be stated that the IRT tests were reliable. In accordance with Table 3, the deviation of the results was low with respect to the average value obtained from the three times series ($\bar{U}$=0.654 W/m^2·K).

As seen in Figure 5, the results of the ACF revealed that some lags fell outside the 95 % confidence interval (2 for 120 minutes, 3 for 60 minutes and 1 for 30 minutes). Nevertheless, these lags did not exceed the expected values (the 5% of the total lags for each test duration). Moreover, no cycles or trends were observed in the three-time series. Only one peak in CP was detected, but it was of minor importance. Hence, it can be affirmed that the measurements can be regarded as a constant signal plus white noise.

An analysis of the graphical representation of 95% confidence intervals (Table 2; Figure 11), revealed that there was no significant difference among the measured U-values for the three test durations. The other statistical parameters related to the variability of the measurements indicated a similar dispersion (Figure 11; Tables 2–3). The standard deviations were found to be between 0.047 W/m^2·K and 0.052 W/m^2·K. The coefficients of variation (CV) ranged from 7.08 % to 8.13 %. In accordance with the aspects described above, the in-situ thermal transmittances of F1 could have been determined after the first 30 minutes of test duration.

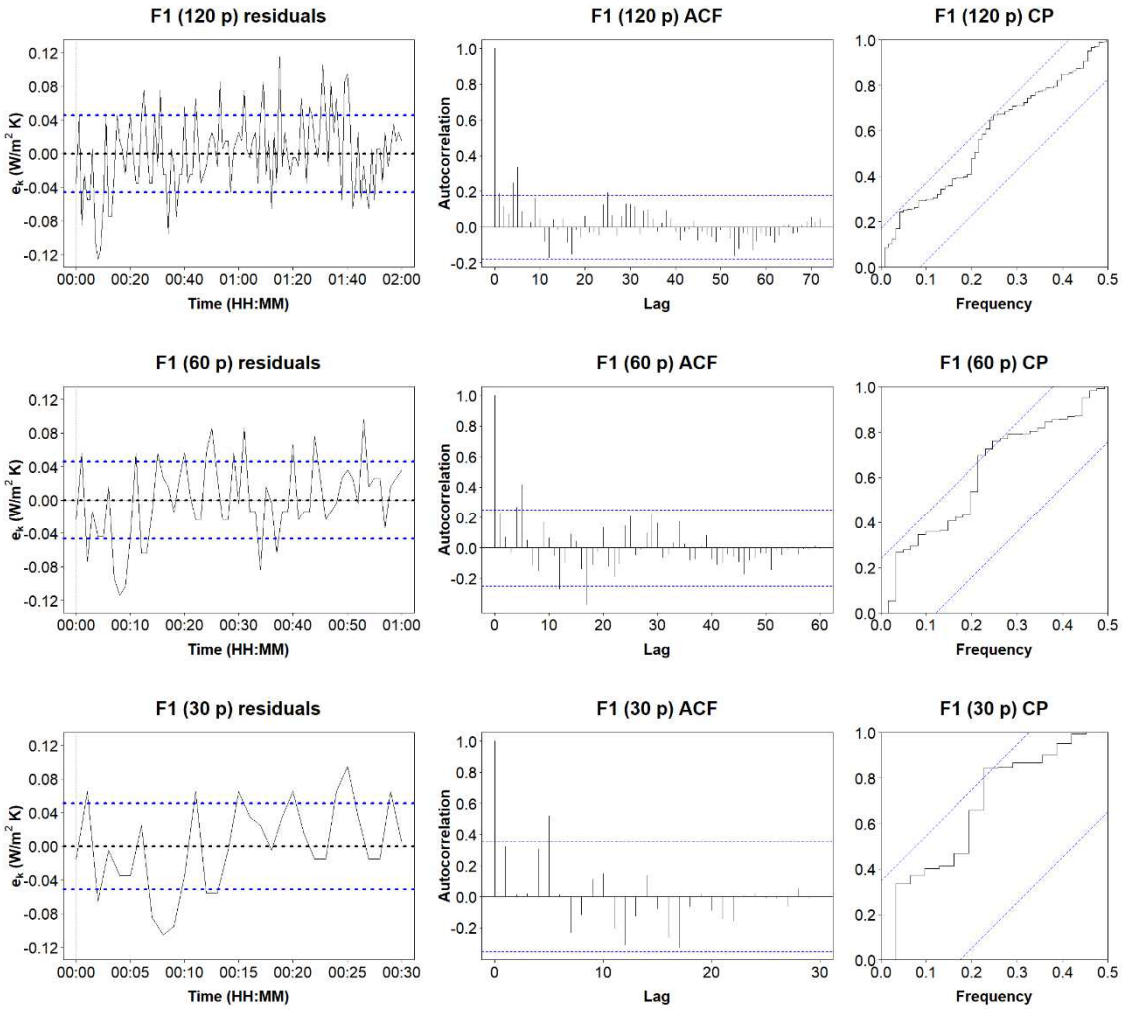

410

411 Figure 5. The left column shows the residuals of the measured data for F1. The middle column presents
412 the ACF plot for F1. The right column indicates the CP for F1

413

414 Most residuals of the quantitative internal IRT measurements of F2 were found to be reliable for the three
415 sampling durations. The average measured U-value of F2 was 0.404 ± 0.053 W/m^2·K (Table 3) and the
416 partial data were: 0.396 W/m^2·K for 120 minutes, 0.399 W/m^2·K for 60 minutes and 0.418 W/m^2·K for
417 30 minutes (Table 2). Hence, the IRT tests can be deemed acceptable. However, the difference between
418 the partial average measured thermal transmittances for 120 and 60 minutes was only 0.003 W/m^2·K,
419 whereas $|\bar{U}_{120} - \bar{U}_{30}|$ increased to 0.022 W/m^2·K (Table 3). Indeed, and considering all façades, this last
420 value was noted as the highest.

421

422 The ACFs did not have a peak and the CPs provided similar information (Figure 6). The values were
423 fitted to the top confidence interval band. Considering the aspects mentioned above, the quantitative

internal IRT measurements of F2 could be accepted as a constant signal plus white noise and a constant sigma independent from the test duration for heavy multi-leaf walls with a low U-value.

An analysis of the variability of measurements obtained for this building envelope (Tables 2-3) indicates that this façade wall had worse standard deviation (σ=0.050–0.056 W/m^2·K) and coefficient of variation (12.70 % < CV < 13.97 %) values than the other investigated samples. There was substantially more variation for the test with 30 data points, as indicated in Figure 11 and Table 3. However, the outcomes of the three test durations might be accepted as valid.

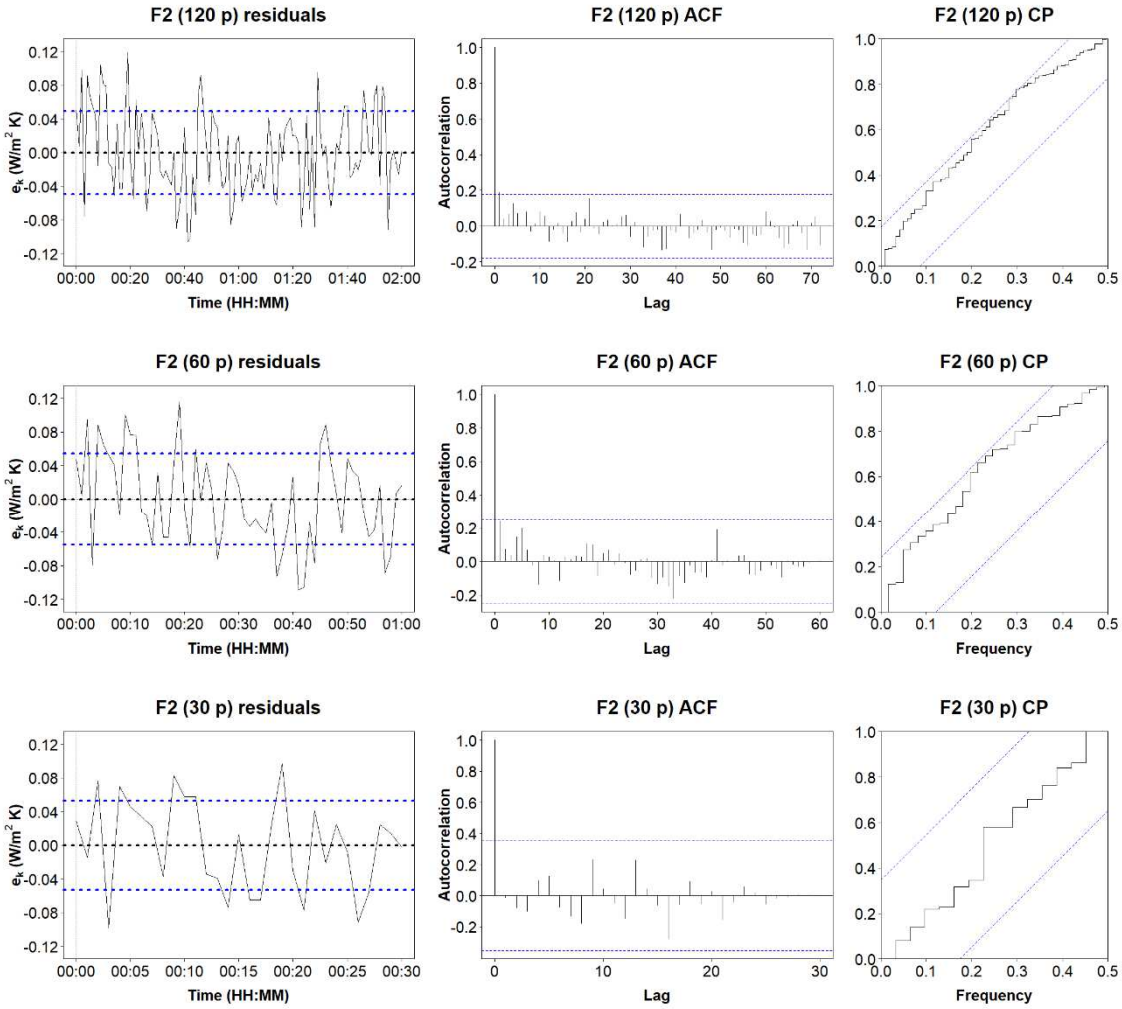

Figure 6. The left column shows the residuals of the measured data for F2. The middle column presents the ACF plot for F2. The right column indicates the CP for F2

The best results were gathered for F3, since the data collected for this building envelope showed extremely similar signals (Table 2): 0.481±0.032 W/m^2·K for 120 minutes; 0.481±0.030 W/m^2·K for 60 minutes; and 0.480±0.031 W/m^2·K for 30 minutes. The deviations among the results were minimal (Table 3) and only four residual peaks presented a value over $e_k = 0 + 0.06$ W/m^2·K (Figure 7).

The above aspects were corroborated with the time series analysis. No significant term was detected in the ACF plots (Figure 7; the middle column). In addition, the CPs of F3 (Figure 7; the right column) were slightly better than the rest of the investigated buildings (the signal described almost a straight line in the middle of the space defined by the two lines of the 95% confidence level band). Hence, it can be affirmed that U-value measurements could be considered a signal with a constant mean plus white noise for each test duration.

Regarding variability (Table 2), the CV was found to be between 6.34% and 6.67%. Therefore, the difference of variability in instantaneous readings was set at 0.24% (Table 3). The standard deviation showed the same value ($\sigma \sim 0.030$ W/m^2·K), regardless of the sampling duration to be validated. These aspects were supported by the graphical representation of the 95% confidence intervals (Figure 5), which were practically the same size. In other words, the same degree of dispersion and skewness was produced in all data. Considering the above aspects, the first 30 minutes of the test might be enough to process the IRT measurements and calculate the thermal transmittance of F3.

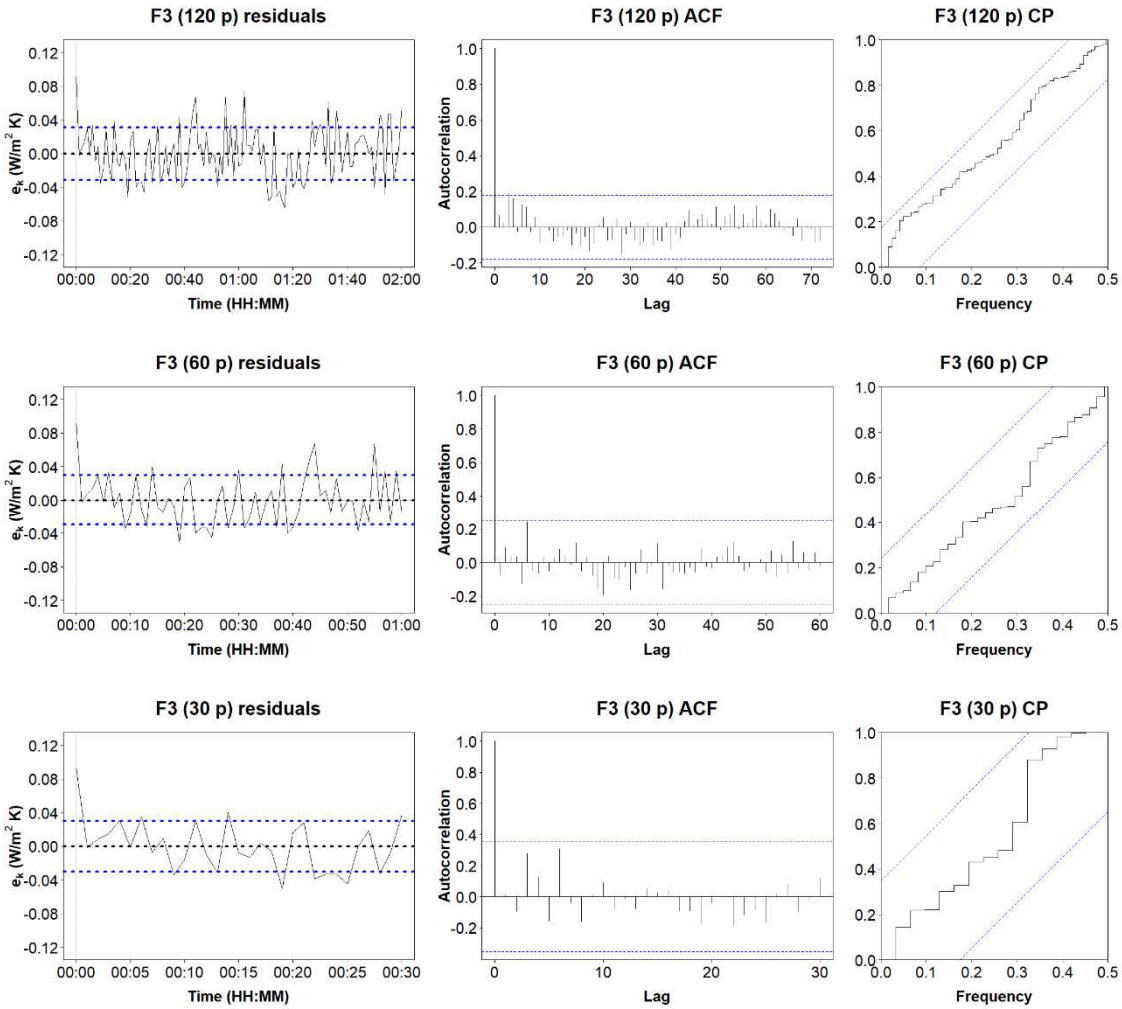

457

458 Figure 7. The left column shows the residuals of the measured data for F3. The middle column presents
459 the ACF plot for F3. The right column indicates the CP for F3

460

461 In the representation of residuals of the U-values for F4 as a function of time (Figure 8), some peaks were
462 distinguished outside of the range [0±σ]. However, they remained under e_k= 0±0.06 W/m^2·K. The
463 partially measured U-values were: 0.430±0.031 W/m^2·K for 120 minutes, 0.431±0.033 W/m^2·K for 60
464 minutes, and 0.425±0.034 W/m^2·K for 30 minutes (Tables 2–3).

465

466 To evaluate in-depth whether the outcomes of this building envelope might be considered reliable, the
467 results needed to be compared with the time series analysis and the study of data variability. In the ACF
468 plot, one significant term was noted for all test durations (Figure 8). In fact, a slight cyclical trend might
469 be described for 60 lags in the graph, but the signals obtained for 120 minutes and 30 minutes discarded
470 this aspect. Practically all readings were inside the 95% confidence interval band, as seen in the CP.

These aspects reveal that the hypothesis of a signal with constant mean plus white noise can be adopted for quantitative IRT measurements. An analysis of variability of the results (Figure 11; Tables 2-3) presented similar standard deviations for all signals (σ=0.031–0.034 W/m^2·K) and coefficients of variation (7.25 % < CV < 8.12 %).

In the graphical representation of the 95% confidence intervals for the U-value estimations (Figure 11), the dispersion of data were slightly higher for the test that took 30 minutes. Overall, the results revealed that the procedure for all tests was correct and the first 30 minutes of the IRT test could be adopted to process the images recorded for F4.

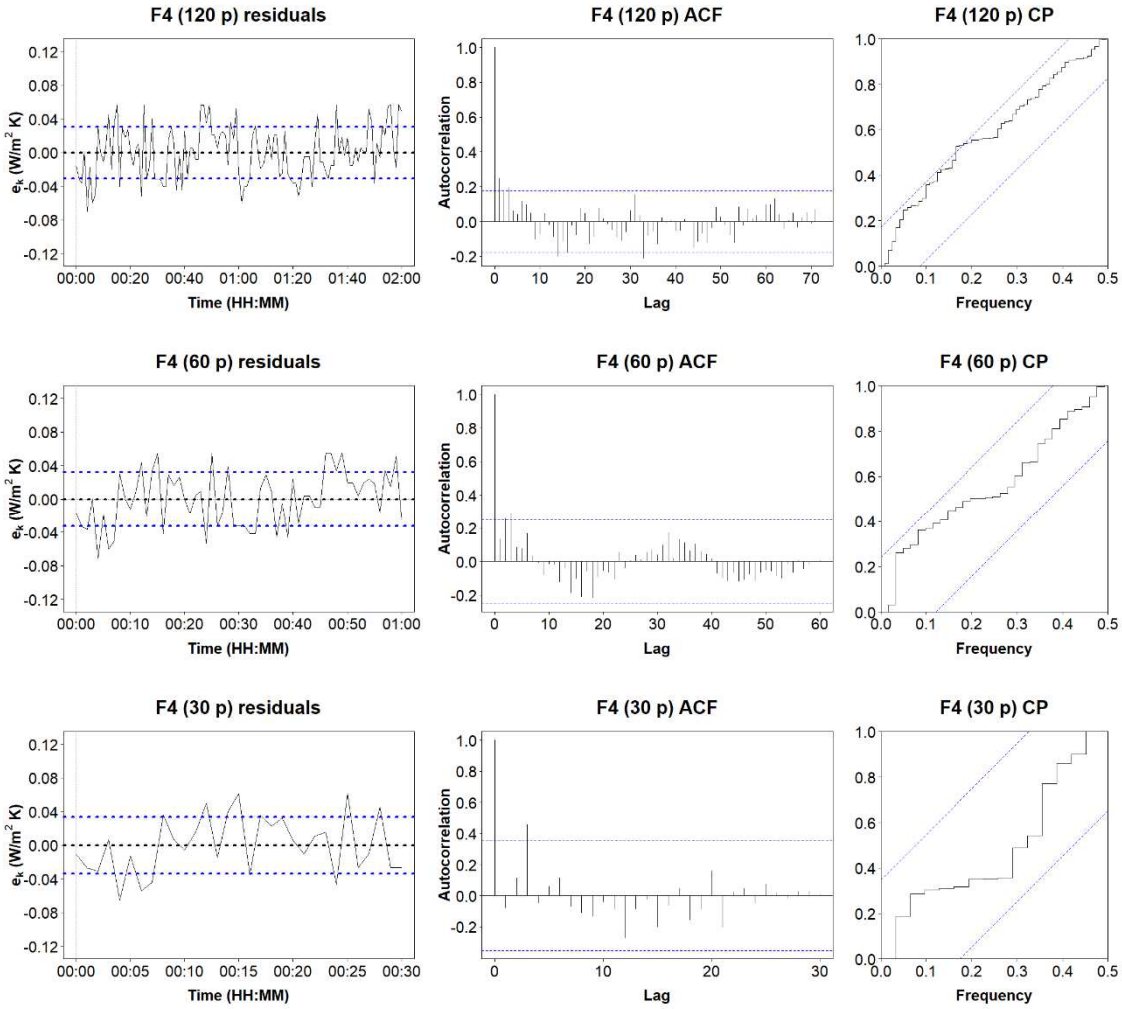

Figure 8. The left column shows the residuals of the measured data for F4. The middle column presents the ACF plot for F4. The right column indicates the CP for F4

Most residuals of U-values for F5 plotted against time were found to be far closer to sigma over the tests. The intervals of the U-value measurements were: 0.557±0.028 $W/m^2 \cdot K$ for 120 minutes; 0.566±0.028 $W/m^2 \cdot K$ for 60 minutes; 0.554±0.031 $W/m^2 \cdot K$ for 30 minutes (Tables 2-3). The statistical parameters were all inside the acceptable range (Table 2), but the data points did not tail away to zero very quickly at the beginning of the tests, especially when the test duration was set at 120 minutes (ACF, Figure 9). Nine significant terms were detected. The residuals of measured U-values fell slightly outside the top band of the 95% confidence interval (CP, Figure 9). The behavior of the signals over time was better for 60 or 30 minutes.

From the analysis of variability (Table 2 and Figure 11), it can be extrapolated that façade F5 had the lowest CV, reaching values between 4.97% and 5.68%. This means that the dispersion of the probability distribution was low. Notably, the difference between the minimum and maximum values of this last statistical parameter was found to be 0.71% (Table 3). The standard deviations were found to be 0.028 $W/m^2 \cdot K$ for 120 and 60 minutes and 0.031 $W/m^2 \cdot K$ for 30 minutes. These facts support the statement that the analysis of thermographic images might be reduced to the first 30 minutes of test duration, as also shown in the graphical representation of 95 % confidence intervals (Figure 11).

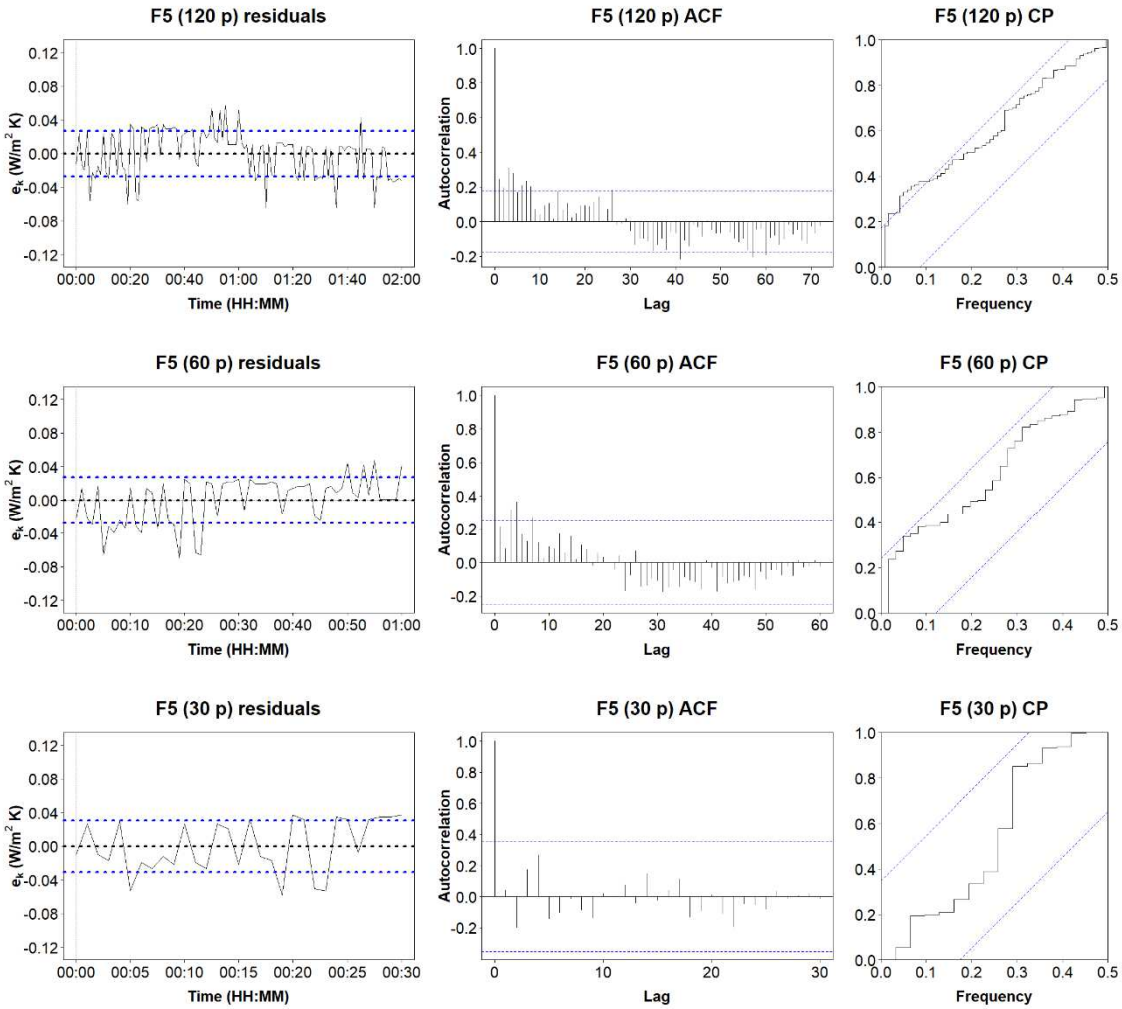

Figure 9. The left column shows the residuals of the measured data for F5. The middle column presents the ACF plot for F5. The right column indicates the CP for F5

In the graphical representation of the residuals of U-values for F6 in function of time (Figure 10), most of the data points showed minor e_k values throughout the tests in comparison with other façades. The average thermal transmittance values were 0.257 W/m^2·K for 120 minutes, 0.260 W/m^2·K for 60 minutes and 0.265 W/m^2·K for 30 minutes (Tables 2-3).

According to Figure 10, some peaks of minor importance were observed in both ACF and CP for 120 points. As seen, measurements could be regarded as a constant mean plus white noise and this façade presented stationarity throughout the tests. In contrast with other heavy multi-leaf walls, some aspects related to the analysis of variability can be highlighted (Tables 2–3). F6 had the lowest values of standard deviation, reaching a maximum value of 0.019 W/m^2·K. The CVs were around 7% like other evaluated

samples, but the variation among partial data was extremely low (0.02 % -Table 3-). Indeed, the results for both statistical parameters were expected, since F6 showed minor residual values (e_k) throughout the tests in comparison with other façades (Figure 10). Considering these aspects, it can be assumed that all the time series defined a signal with constant mean plus white noise and the hypothesis of stationarity can be fulfilled.

Concerning the graphical representation of the 95% confidence intervals (Figure 11), the outcomes showed a downward trend of the average measured U-value and its confidence intervals were far smaller for a longer sampling duration. Therefore, only the first 30 minutes of the test might be required to determine the in-situ measured U-value.

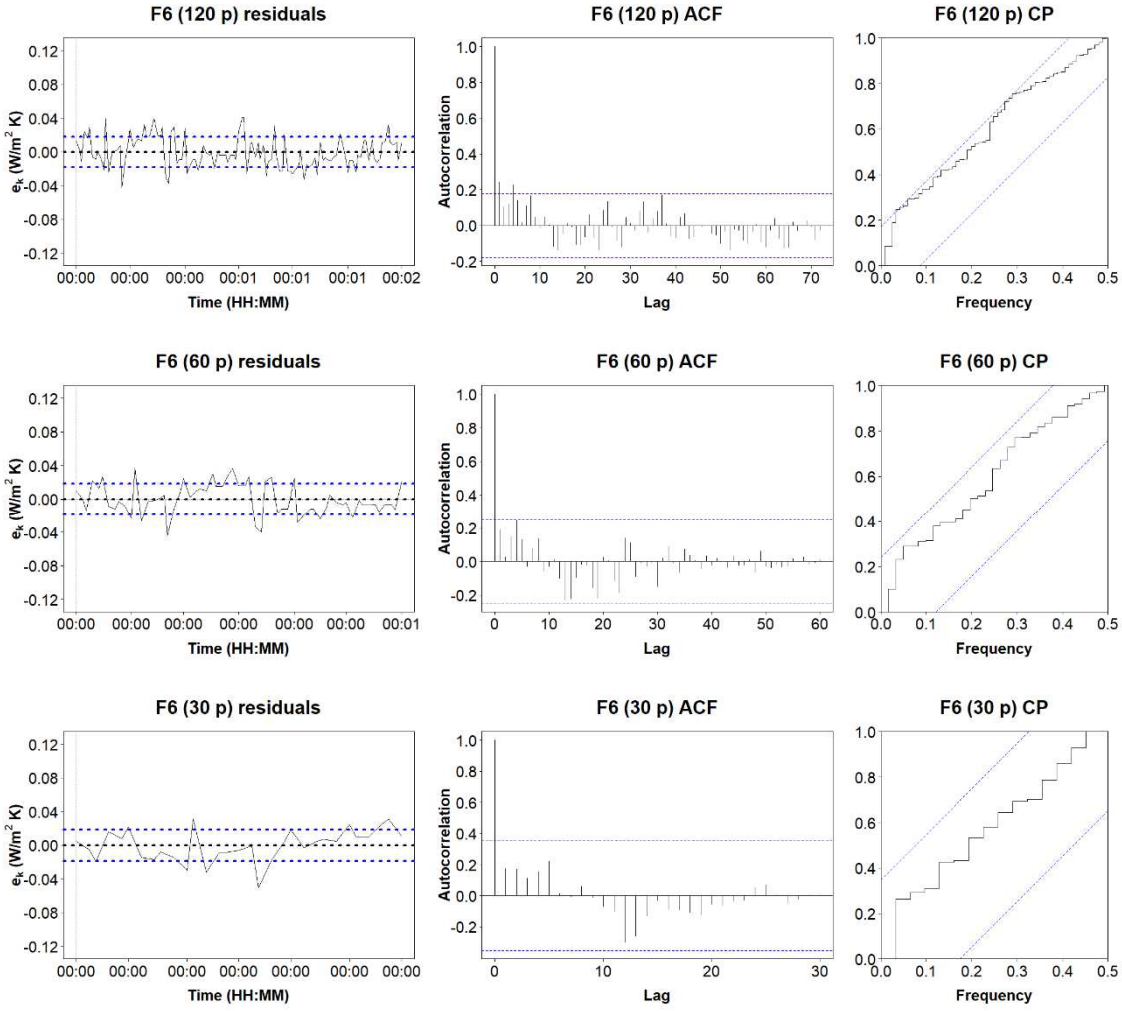

Figure 10. The left column shows the residuals of the measured data for F6. The middle column presents the ACF plot for F6. The right column indicates the CP for F6

Overall, it can be concluded that all statistical results reported reasonable values. Hence, it can be stated that the first 30 minutes of the test might be enough to determine in-situ measured U-values. The proposed hypothesis for the U-values time series analysis was fulfilled for all investigated samples, to obtain a signal with a constant mean plus white noise. This aspect was in line with the results of the ACF and CP plots, where some lags fell outside the 95% confidence interval but were less than 5% (Figures 5–10).

The graphical representation of the 95% confidence intervals of all investigated façades suggested that the variability in the measurements did not differ significantly among the three selected sampling durations (Table 2–3; Figure 11). In fact, confidence intervals were extremely similar among samples (i.e. F1 and F2; F3 to F6) and were slightly greater for 30 points. This last aspect was expected due to a reduction in the sample size for the time series. In other words, the confidence interval is defined as CI = f ($\bar{U}$, σ, n) in accordance with Section 2.2. If the mean and sigma remained practically constant among tests, the only parameter that entailed an increase or decrease in CI length was the number of thermograms to be analysed. Moreover, the comparative analysis among sigma values gathered for each time series (Table 3) showed that the differences ranged around zero, reaching 0.005 $W/m^2 \cdot K$ as a maximum. The CVs were also low (from 4.97 to 8.13% for façades F1, F3–F6), except façade F2 (12.70 to 13.97%). As seen in Table 3, the differences in CVs among time series were found to be under 1% in most cases. A thorough literature review showed that quantitative internal IRT did not have a limit for the CV. Nevertheless, the results of this research were consistent with previous studies on other techniques, such as the standardized HFM method [9, 11, 118, 45, 12, 13, 32, 15, 119]. Considering all the aspects mentioned above, it could be stated that a longer test duration would not lead to an improvement in results.

560 Table 2. Summary of results. Average measured U-values (Ū), standard deviation (σ), coefficient of
561 variation (CV) and validation of the hypothesis of a constant signal plus white noise

	ΔT [°C]	Time [min]	Ū [W/m²·K]	σ [W/m²·K]	CV [%]	Hypothesis
F1	6.80 <ΔT < 8.70	120	0.665	0.047	7.08	Fulfilled
		60	0.654	0.047	7.29	Fulfilled
		30	0.645	0.052	8.13	Fulfilled
F2	7.60 <ΔT < 9.10	120	0.396	0.050	12.70	Fulfilled
		60	0.399	0.056	13.97	Fulfilled
		30	0.418	0.054	12.99	Fulfilled
F3	5.80 <ΔT < 8.20	120	0.481	0.032	6.67	Fulfilled
		60	0.481	0.030	6.34	Fulfilled
		30	0.480	0.031	6.42	Fulfilled
F4	8.70 <ΔT < 9.60	120	0.430	0.031	7.25	Fulfilled
		60	0.431	0.033	7.69	Fulfilled
		30	0.425	0.034	8.12	Fulfilled
F5	18.30 <ΔT< 19.60	120	0.557	0.028	4.97	Fulfilled
		60	0.566	0.028	5.02	Fulfilled
		30	0.554	0.031	5.68	Fulfilled
F6	8.20 <ΔT < 10.40	120	0.257	0.018	7.16	Fulfilled
		60	0.260	0.019	7.32	Fulfilled
		30	0.265	0.019	7.18	Fulfilled

562

563

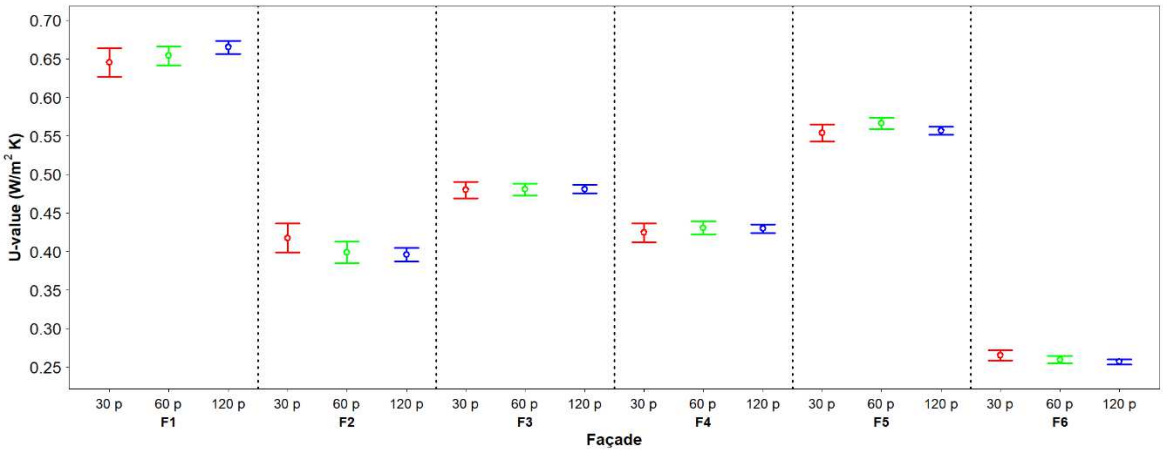

564

565 Figure 11. Graphical representation of 95% confidence intervals for U-value estimations

566 Table 3. Estimation of variability

	F1	F2	F3	F4	F5	F6
Estimation $\bar{U}$ [W/m^2·K]	0.654	0.404	0.480	0.428	0.559	0.261
$\lvert \bar{U}_{120} - \bar{U}_{60} \rvert$	0.011	0.003	0.000	0.001	0.010	0.003
$\lvert \bar{U}_{60} - \bar{U}_{30} \rvert$	0.009	0.019	0.001	0.006	0.012	0.006
$\lvert \bar{U}_{120} - \bar{U}_{30} \rvert$	0.020	0.022	0.001	0.005	0.003	0.008
Estimation σ [W/m^2·K]	0.049	0.053	0.031	0.033	0.029	0.019
$\lvert \sigma_{120} - \sigma_{60} \rvert$	0.000	0.005	0.002	0.002	0.001	0.001
$\lvert \sigma_{60} - \sigma_{30} \rvert$	0.005	0.001	0.000	0.001	0.003	0.000
$\lvert \sigma_{120} - \sigma_{30} \rvert$	0.005	0.004	0.001	0.003	0.004	0.001
Estimation coefficient of variation [%]	7.49	13.22	6.48	7.69	5.22	7.22
$\lvert CV_{120} - CV_{60} \rvert$	0.18	1.27	0.33	0.43	0.04	0.16
$\lvert CV_{60} - CV_{30} \rvert$	0.87	0.97	0.09	0.43	0.66	0.13
$\lvert CV_{120} - CV_{30} \rvert$	1.05	0.29	0.24	0.87	0.70	0.02

567

568

569 **3.3. U-value time series analysis by signal modelling technique**

570 As mentioned above (Section 2.3), a second U-value time series analysis was conducted in this study
571 using the MATLAB "System Identification Toolbox" [75] to support the results obtained by the first U-
572 value time series analysis through statistical tests (Section 3.2). The MATLAB are detailed below.

573

574 The results revealed that the models with the best adjustment for the reference signal were ARX or
575 ARMX. The model was stable for all heavy multi-leaf walls if it was constituted by a simple structure
576 (*na*=1, *nb*=4, *nk*=7). According to Jiménez et al. [109], *na* denotes the order of polynomial *A(q)*, *nb* the
577 order of polynomial *B(q)*, and *nk* the delay between output and input. In this thesis, the analysis was
578 limited to models with *na*, *nb* and *nk*, varying between 1 and 10. By way of example, the results of façade
579 F3 are presented. Figure 12 shows the typical model structure for this building envelope. The models
580 indicated as "Best Fit" (red) by the "System Identification Tool" were those characterized by *na=10*, *nb=*
581 *10* and *nk=8*. Nevertheless, the MDL Choice (green) was enough for this study, since the biggest change
582 in the model misfit was generated at the beginning and provided less complexity in the execution.

583

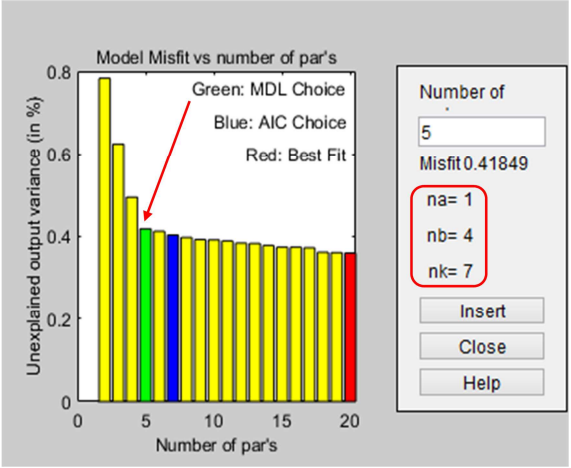

584

585 Figure 12. Façade 3. ARX model structure

586

587 According to Figure 13, the model ARX was stable since all zeros and pols were located inside the unit
588 circle. The frequency function does not show signals of instability for a simple model structure. However,
589 several peaks of resonance were detected as the complexity of the model increased (Figure 14), when the
590 structure of the red bar (Figure 12) was chosen. In the ACF of the residuals, all observations were inside
591 the 95% confidence interval bands (Figure 15).

592

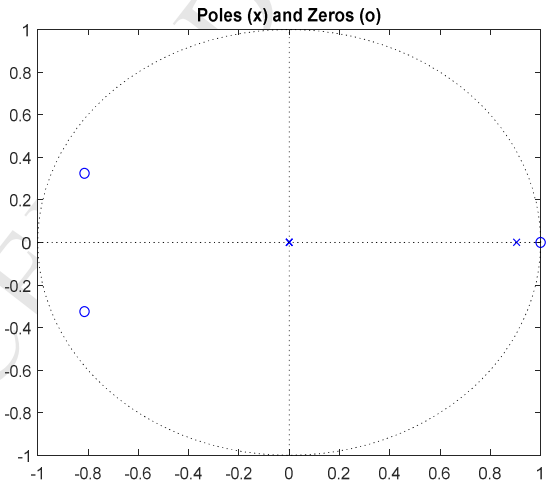

593

594 Figure 13. Zeros and poles plot for façades F3

595

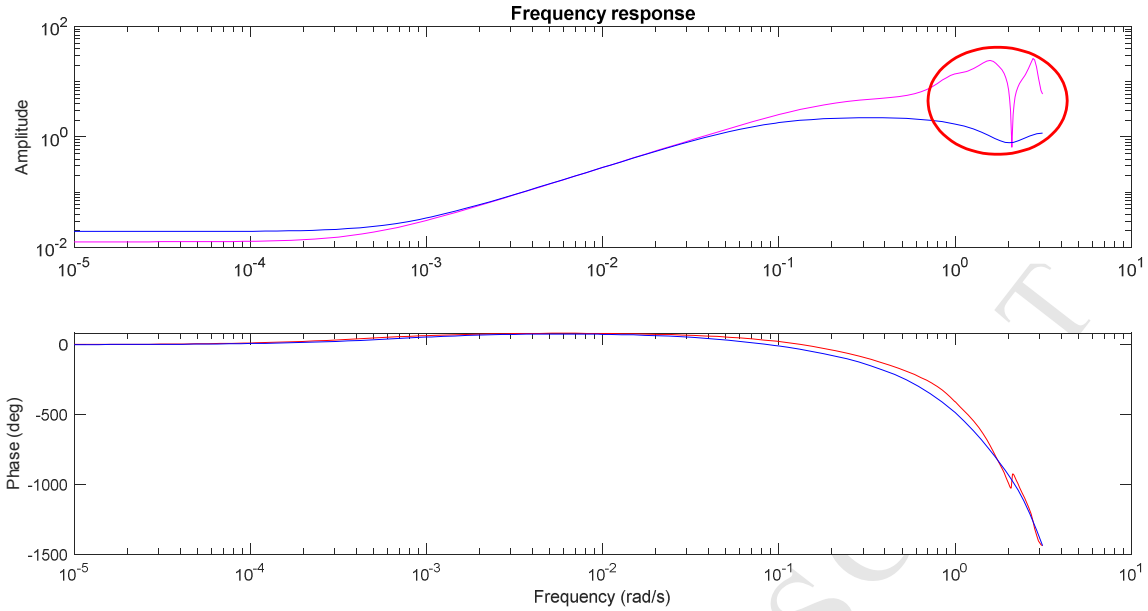

596

597 Figure 14. Frequency response for F3. Peaks of resonance when the complexity of the model increased

598

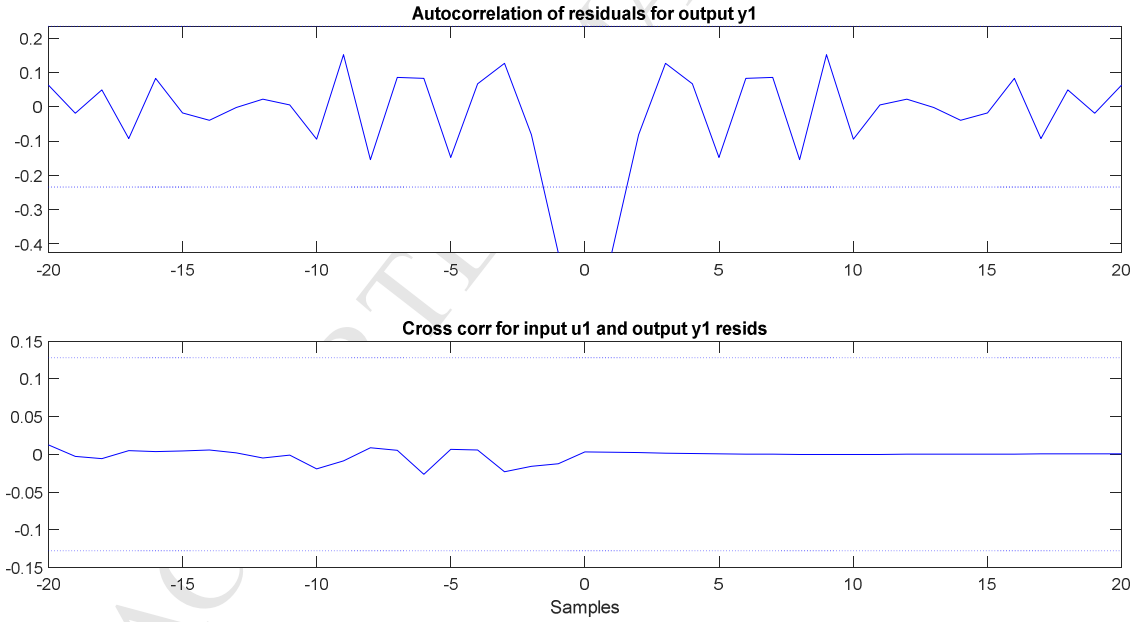

599

600 Figure 15. ACF of residuals for façades F3

601

602 As regards the comparative analysis between the developed signal models and IRT measurements, the
603 results are shown in Figures 17–22 and Table 4. In the plots, it can be observed that: the theoretical
604 thermal transmittance and the margin of error (±5%) were indicated with a discontinuous red line; the
605 measured IRT signal was drawn in black; and the modelled signal was represented in different colours to

illustrate the behaviour of each wall when the second U-value time series analysis was applied. MATLAB ensured that the system was an under stationary regime for all investigated buildings. In addition, the modelled signals were practically stable and continuous for 30≤N≤120 (Figures 17 to 22). Hence, and as the first U-value time series analysis had shown previously (Section 3.2), short-lasting tests could be executed.

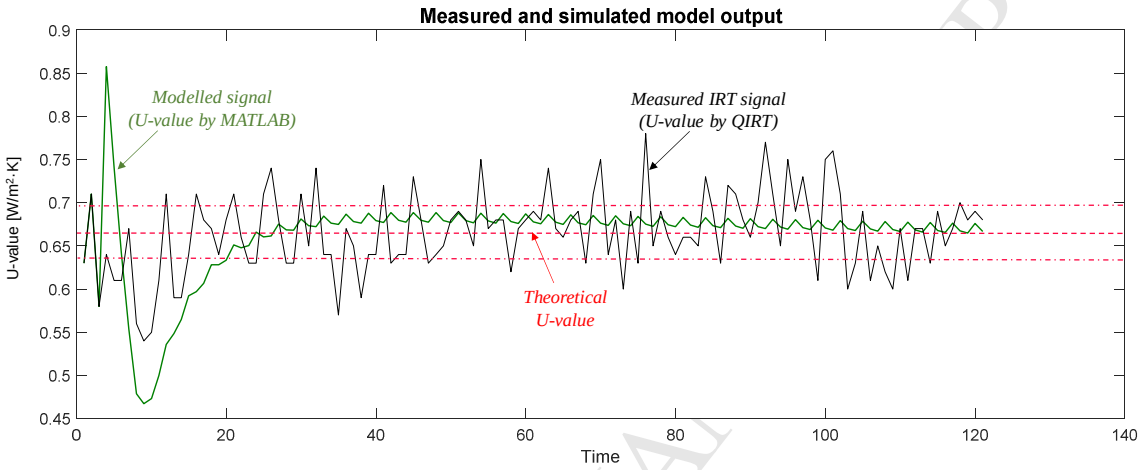

Figure 16. Façade 1. IRT measurements, theoretical U-value and MATLAB modelled signal

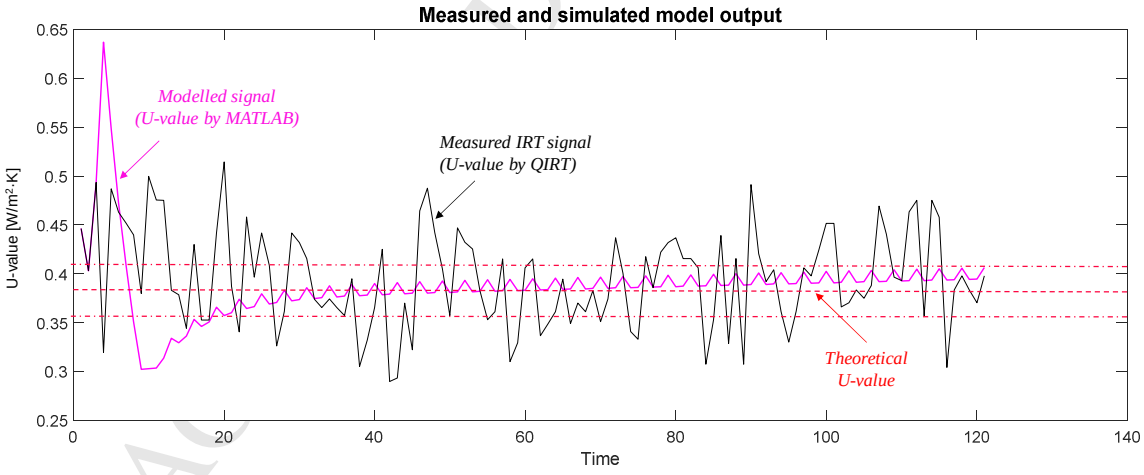

Figure 17. Façade 2. IRT measurements, theoretical U-value and MATLAB modelled signal

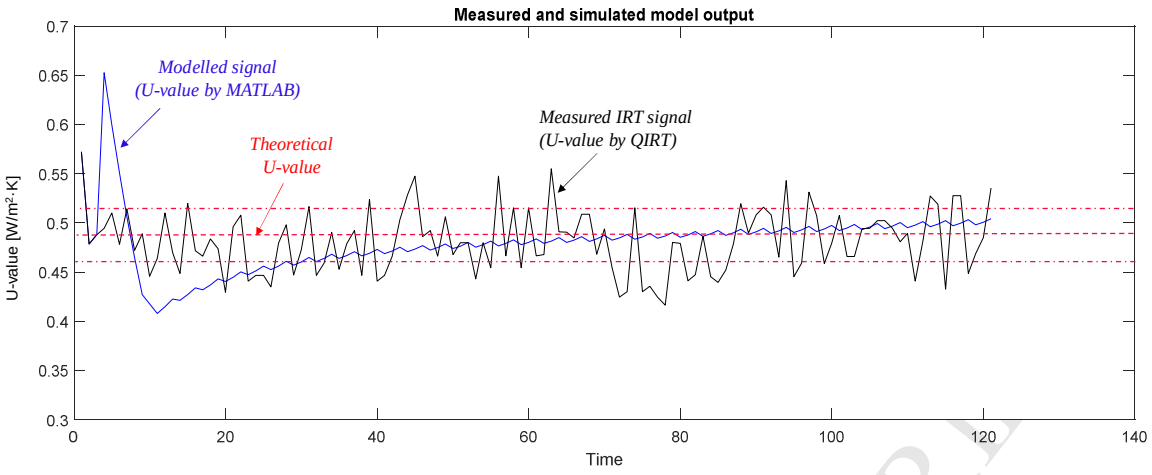

618

619 Figure 18. Façade 3. IRT measurements, theoretical U-value and MATLAB modelled signal

620

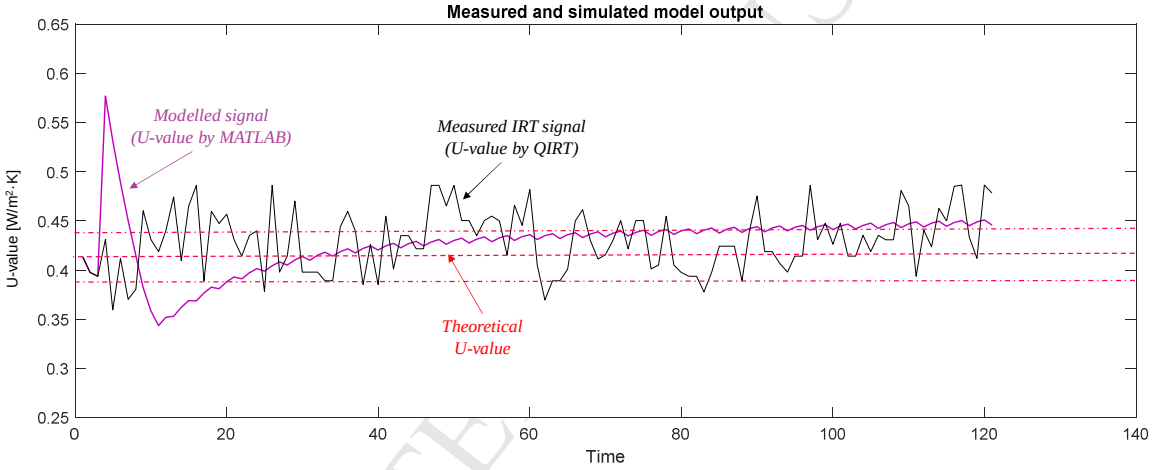

621

622 Figure 19. Façade 4. IRT measurements, theoretical U-value and MATLAB modelled signal

623

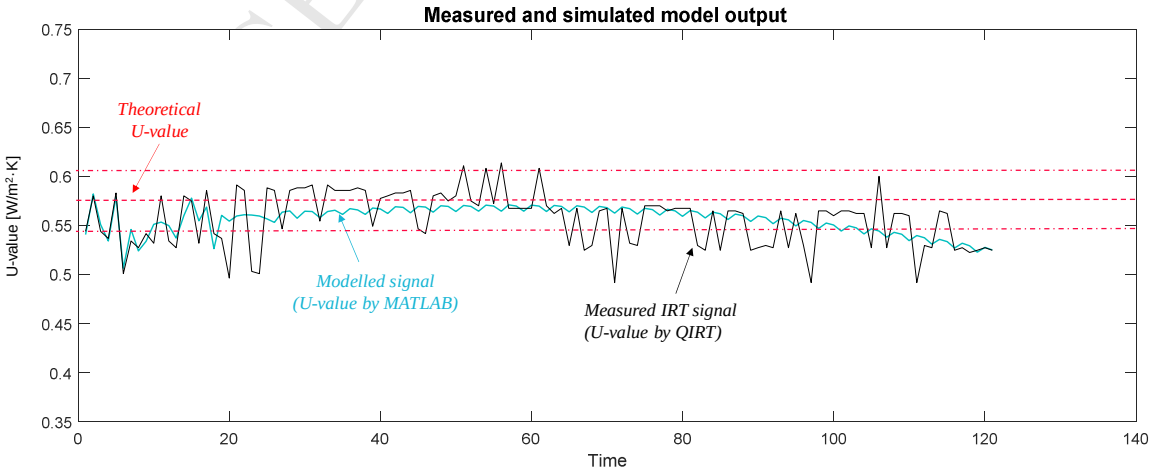

624

625 Figure 20. Façade 5. IRT measurements, theoretical U-value and MATLAB modelled signal

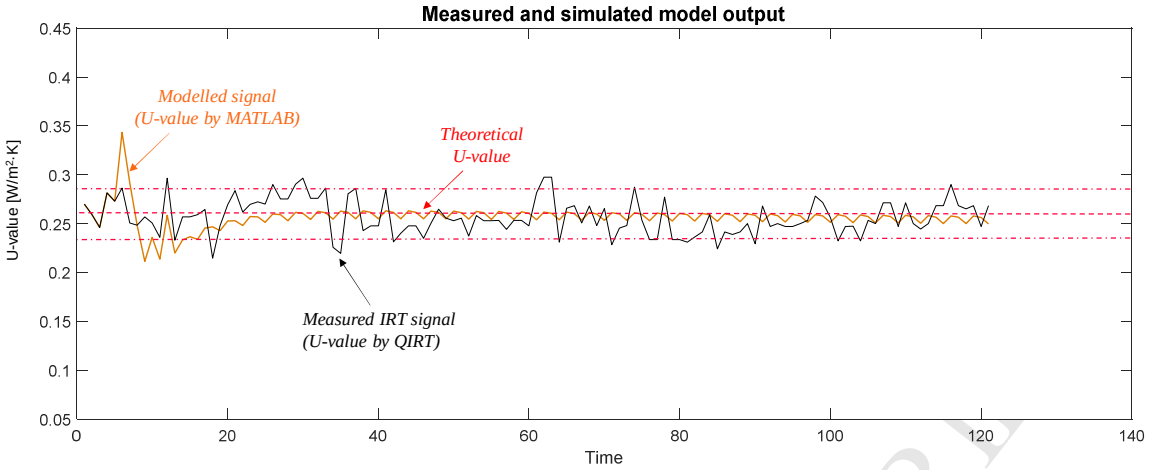

Figure 21. Façade 6. IRT measurements, theoretical U-value and MATLAB modelled signal

Besides this, the thermal transmittances estimated by the MATLAB ARX model and those obtained by the quantitative internal IRT method did not differ significantly among the three sampling durations. Indeed, the deviations between the theoretical and the MATLAB modelled signal ($\Delta U_1/U_t$) as well as the deviations between the theoretical and the QIRT measured signal ($\Delta U_2/U_t$) were found to be under 10% (Table 4; F1, F3 to F6). Therefore, the IRT survey could be stopped earlier than previous researches had adopted in the last few decades, since the errors are within an acceptable range.

Tejedor et al. [56] stated that heavy multi-leaf walls with low U-values might be difficult to measure. With the current research, it was observed that heavy multi-leaf walls with a low thermal transmittance and low heat capacity per unit of area (i.e. F2 and F6) require further research. As seen in Table 4, some discrepancies in terms of thermal behaviour were detected. In contrast to F6, where the deviations $\Delta U_1/U_t$ and $\Delta U_2/U_t$ were similar, F2 reached a deviation $\Delta U_2/U_t$ around 15% for the measured IRT signal and a deviation $\Delta U_1/U_t$ under 9% for the modelled signal. Therefore, the assembly of the wall layers and /or the type of material could play a greater impact on determination of the measured U-value than the test duration.

649 Table 4. Comparative analysis of modelled and original IRT signals

Case Studies	Time [min]	Modelled signal (MATLAB) U_{MODEL} [W/m²·K]	Measured signal (QIRT) U_{MES_AVG} [W/m²·K]	Theoretical U-value (Standards) U_t [W/m²·K]	$\Delta U_1/Ut$ [%]	$\Delta U_2/Ut$ [%]
F1	120	0.675	0.665	0.657	2.74	1.22
	60	0.687	0.654		4.57	0.46
	30	0.681	0.645		3.65	1.83
F2	120	0.394	0.396	0.362	8.84	9.39
	60	0.383	0.399		5.80	10.22
	30	0.374	0.418		3.31	15.47
F3	120	0.497	0.481	0.480	3.54	0.21
	60	0.484	0.481		0.83	0.21
	30	0.468	0.480		2.50	0.00
F4	120	0.461	0.430	0.420	9.76	2.38
	60	0.455	0.431		8.33	2.62
	30	0.430	0.425		2.38	1.19
F5	120	0.550	0.557	0.586	6.14	4.95
	60	0.562	0.566		4.10	3.41
	30	0.545	0.554		5.46	5.46
F6	120	0.256	0.257	0.252	1.59	1.98
	60	0.260	0.260		3.17	3.17
	30	0.260	0.265		3.17	5.16

650

651 *U_{MODEL}: modelled signal of thermal transmittance estimated by the MATLAB ARX model; U_{MES_AVG}: measured thermal transmittance*
652 *determined by quantitative internal IRT following Section 3.2; U_t: theoretical thermal transmittance; $\Delta U_1/U_t$: deviation between the*
653 *theoretical and modelled U-value; $\Delta U_2/U_t$: deviation between the theoretical and measured U-value*

654

655 Notably, the U-value of Façade F5 was significantly underestimated for both the modelled and measured
656 IRT signal. In this occupied residential building, the temperature difference (ΔT) ranged from 18.30ºC to
657 19.60ºC. According to Tejedor et al. [56], the variance of the measured U-value could be attributed to
658 changes in the wall surface temperature (T_{WALL}) when 16ºC <ΔT < 21ºC, reaching deviations of the
659 measured U-value of around -15%. Hence, aspects related to the influence of operating conditions on the
660 determination of the thermal transmittance of the current research were consistent with previous studies.

661

662

3.4. Proposal for stopping IRT tests

According to the comparative analysis of Section 3.3., and in terms of applicability, a routine in basis on statistical tests could be proposed to stop quantitative IRT tests (Figure 22). It was demonstrated that algorithms focused on statistical analysis (i.e. ACF and CP) might be more reliable and accurate than those mathematical procedures based on modelled signals (Table 4).

Future automation of the system could consist of adding one thermographic image each t+1' once the premise of N≥30 has been reached. As represented in Figure 22, the algorithm is initiated by implementation of the quantitative internal IRT method. The measuring equipment monitors and records environmental conditions (inner and outer air ambient temperature) and the parameters related to the façade (ε_{WALL}, T_{WALL} and T_{REF}). With a minimum time delay, a first data package of 30 measurements (one image per minute) will be introduced into the numerical model to determine in-situ instantaneous thermal transmittances. To fulfil the hypothesis (*U-value is a constant signal plus white noise*) and stop the IRT survey, the residuals of the measured signal should be located inside the 95% confidence interval bands for the ACF and CP. Regarding variability among IRT measurements and after calculating the statistical parameters specified in Section 2.2, CV should be ≤ 10% and σ should range between 0.01 and 0.05 W/m^2·K. Otherwise, one image needs to be added to the routine.

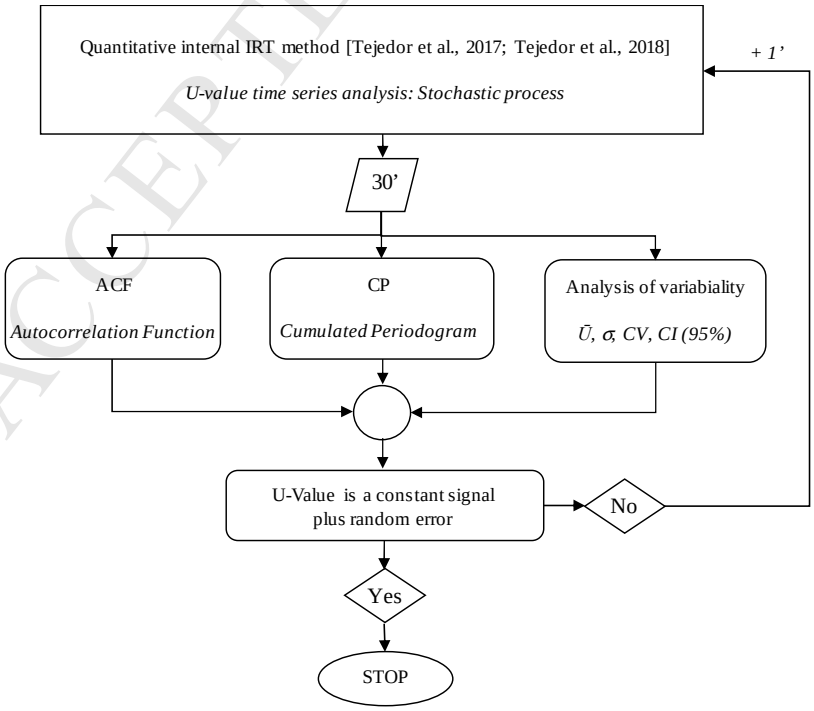

Figure 22. Flowchart of the routine for stopping IRT tests

4. CONCLUSIONS

In the recent decades, the usual approach adopted for this NDT is based on manually post-processing from 120 to 7200 thermograms for data acquisition intervals of 1 minute to 1 second respectively. This entails both a reduction of effectiveness and a lack of robustness to determine the measured thermal transmittance.

For the first time, a research allowed to demonstrate the feasibility of performing short-lasting IRT tests by means of two U-value time series analyses (statistical tests and the MATLAB signal modelling technique). The main reasons are exposed as follows. Firstly, no significant differences were detected among sampling durations (30, 60 and 120 minutes) for the estimation of in-situ thermal transmittance. Hence, long-lasting tests do not necessarily lead to lower errors, in contrast to the usual assumption about test duration adopted in previous studies. Secondly, the number of quantitative IRT measurements could be reduced in all investigated buildings and consequently, reliable U-values could be achieved in a shorter analysis time. Thirdly, the IRT test could be stopped earlier (from 30 minutes). As a conclusive remark, this research underlined that techniques such as ACF or CP and signal modelling by MATLAB can be used to verify whether non-transient conditions have been fulfilled during on-site construction surveys.

The findings also suggested that the sampling duration might be a minor source of discrepancy in the determination of measured U-values, compared to the influence of operating conditions and thermophysical properties reported by Tejedor et al. [56].

In terms of applicability, this research leads us to propose an innovative data management tool for stopping quantitative IRT tests when the results of the measured U-value present a high trustworthiness. The routine should be focused on assuming instantaneous measured thermal transmittances as a stochastic process constituted by a constant signal plus white noise, regardless of the internal wall configuration.

This aforementioned proposal could allow the NDT to be automated in the mid-term, helping to advance the standardization of quantitative IRT for heavy multi-leaf walls: (i) a common measurement pattern could be drawn up; (ii) the data analysis could be simplified. In this way, the entire procedure would become more efficient and could be incorporated into the industrial market as a building diagnosis tool to

facilitate decision –making in real built environments. Tests of 120 minutes might be used in energy audit procedures while tests of 30 minutes could be implemented to evaluate the state of the building in a walk-through survey in terms of periodic maintenance controls. Nevertheless, further research is required to analyse more wall types and the influence of climate on external façades or observe if future studies by other researchers are in line with the conclusions posed in this journal paper.

ACKNOWLEDGEMENTS

The authors would like to thank the Industrial Engineers' Institution of Catalonia and Terrassa City Council for promoting this research. The authors also express their gratitude to the Department of Housing and Urban Development of Terrassa for allowing access to council-owned buildings. Finally, the authors acknowledge Evowall Technology for allowing measurement of the building mock-up with a low U-value and for facilitating the monitoring process.

CONFLICT OF INTEREST

The authors have no conflict of interest

REFERENCES

[1] Emmel, M.G; Abadie, M.O.; Mendes, N. *New external convective heat transfer coefficient correlations for isolated low -rise buildings*. Energy and Buildings 39 (2007) 335-342

[2] Prada, A; Cappelletti, F; Baggio, P; Gasparella, A. *On the effect of material uncertainties in envelope heat transfer simulations*. Energy and Buildings 71 (2014) 53-60

[3] Rossi, M; Rocco, V.M. *External walls design: The role of periodic thermal transmittance and internal areal heat capacity*. Energy and Buildings 68 (2014) 732 -740

[4] Liu, J; Heidarinejad, M; Gracik, S; Srebric, J. *The impact of exterior surface convective heat transfer coefficients on the building energy consumption in urban neighbourhoods with different plan area densities.* Energy and Buildings 86 (2015) 449-463

[5] Asdrubali, F; Baldinelli, G; Bianchi, F. *A quantitative methodology to evaluate thermal bridges in buildings.* Applied Energy 97 (2012) 365-373

[6] Vereecken, E; Roels, S. *A comparison of the hygric performance of interior insulation systems: A hot box-cold box experiment.* Energy and Buildings 80 (2014) 37-44

[7] Kumar, A; Suman, B.M. *Experimental evaluation of insulation materials for walls and roofs and their impact on* indoor *thermal comfort under composite climate*. Building and Environment 59 (2013) 635-643

[8] Anderson, B.R. *The measurement of U-values on site*. Proceedings of the ASHRAE/DOE/BTECC Conference (1985)

[9] Roulet, C; Gass, J; Markus, I. *In-situ U-value measurement: reliable results in short time by dynamic interpretation of measured data*. Proceedings Thermal Performance of the Exterior Envelopes of Buildings III. ASHRAE (1985) 777-784

[10] Flanders, S.N. *In-situ Heat Flux Measurements in Buildings. Applications and Interpretations of Results*. CRREL Special Report 91-3, U.S. Army Corps of Engineers, Cold Regions Research and Engineering Laboratory (1991)

[11] Flanders, S.N. *The convergence criterion in measuring building R-values*. Proceedings Thermal Performance of the Exterior Envelopes of Buildings V. ASHRAE (1992) 204-209

[12] Ahmad, A; Maslehuddin, M; Al-Hadhrami, L.M. *In situ measurement of thermal transmittance and thermal resistance of hollow reinforced precast concrete walls.* Energy and Buildings 84 (2014) 132 -141

[13] Ficco, G; Iannetta, F; Ianniello, E; d'Ambrosio, F.R.; Dell'Isola, M. *U-Value in situ measurement for energy diagnosis of existing buildings.* Energy and Buildings 104 (2015) 108-121

773 [14] Gaspar, K; Casals, M; Gangolells, M. *A comparison of standardized calculation methods for in situ*
774 *measurements of façades U-value*. Energy and Buildings 130 (2016) 592-599
775
776 [15] Atsonios, I.A.; Mandilaras, I.O; Kontogeorgos, A.D.; Founti, M.A. *A comparative assessment of the*
777 *standardized methods for the in-situ measurement of the thermal resistance of building walls*. Energy and
778 Buildings 154 (2017) 198-206
779
780 [16] Anderson, L.J. *Energy conservation with thermography*. Proceedings of the Infrared Information
781 Exchange. AGA Corporation (1977) 61-62
782
783 [17] Burch, D.M; Kusuda, T; Blum, D.G. *An infrared technique for heat loss measurement*. NBS
784 Technical Note 933, U.S. Government Printing Office (1977)
785
786 [18] Burn, K; Schuyler, G. *Applications of infrared thermography in locating and identifying building*
787 *faults*. Journal of International Institute for Conservation 4 (1980) 3-14
788
789 [19] Flanders, S.N; Marshall, S.J. *Interpolating R-Values from thermograms*. Proceedings of
790 Thermosense IV, SPIE –The International Society for Optical Engineering- (1981) 157-164
791
792 [20] McIntosh, G.B. *Recent advances in the quantification of heat loss using thermography*. Proceedings
793 of Thermosense IV, SPIE –The International Society for Optical Engineering- (1981) 213-218
794
795 [21] Straube, J; Burnett, E.F.P. *Rain control and design strategies*. Journal of Building Physics 23 (1999)
796 41-56
797
798 [22] Kalamees, T. *Air tightness and air leakages of new lightweight single-family detached houses in*
799 *Estonia*. Building and Environment 42 (2007) 2369-2377
800
801 [23] Madding, R. *Finding R-values of stud frame constructed houses with IR thermography*. Proceedings
802 of InfraMation (2008)

[24] Lucchi, E. *Non-invasive method for investigating energy and environmental performances in existing buildings*. PLEA Conference on Passive and Low Energy Architecture (2011)

[25] Taylor, T; Counsell, J; Gill, S. *Energy efficiency is more than skin deep: Improving construction quality control in new-building housing using thermography*. Energy and Buildings 66 (2013) 222-231

[26] Meola, C; Carlomagno, G.M. *Infrared thermography to evaluate impact damage in glass/epoxy with manufacturing defects*. International Journal of Impact Engineering 67 (2014) 1-11.

[27] Fox, M; Coley, D; Goodhew, S; de Wilde, P. *Time- lapse thermography for building defect detection.* Energy and Buildings 92 (2015) 95-106

[28] Barreira, E; Almeida, R.M.S.F; Delgado, J.M.P.Q. *Infrared thermography for assessing moisture related phenomena in building components.* Construction and Building materials 110 (2016) 251-269

[29] Lehman, B; Ghazi Wakili, K; Frank, Th; Vera Collado, B; Tanner, Ch. *Effects of individual climatic parameters on the infrared thermography of buildings*. Applied Energy 110 (2013) 29-43

[30] Tzifa, V; Papadakos, G; Papadopoulou, A.G.; Marinakis, V; Psarras, J. *Uncertainty and method limitations in a short-time measurement of the effective thermal transmittance on a building envelope using an infrared camera*. International Journal of Sustainable Energy (2014) 1-19

[31] Albatici, R; Tonelli, A.M.; Chiogna, M. *A comprehensive experimental approach for the validation of quantitative infrared thermography in the evaluation of building thermal transmittance*. Applied Energy 141 (2015) 218-228

[32] Meng, X; Yan, B; Gao, Y; Wang, J; Zhang, W; Long, E. *Factors affecting the in-situ measurement accuracy of the wall heat transfer coefficient using the heat flow meter method*. Energy and Buildings 86 (2015) 754-765

[33] Nardi, I; Paoletti, D; Ambrosini, D; de Rubeis, T; Sfarra, S. *U-Value assessment by infrared thermography: A comparison of different calculation methods in a Guarded Hot Box*. Energy and Buildings 122 (2016) 211-221

[34] O'Grady, A.M.; Lechowska, A.A; Harte, A.M. *Quantification of heat losses through building envelope thermal bridges influenced by wind velocity using the outdoor infrared thermography technique*. Applied Energy 108 (2017) 1038 – 1052

[35] Haralambopoulos, D; Paparsenos, G.F. *Assessing the thermal insulation of old buildings –The need for in-situ spot measurements of thermal resistance and planar infrared thermography*. Energy Conversion and Management 39 (1998) 65-79

[36] Albatici, R; Tonelli, A.M. *Infrared thermovision technique for the assessment of thermal transmittance value of opaque building elements on site*. Energy and Buildings 42 (2010) 2177-2183

[37] Kisilewicz, T; Wróbel, A. *Quantitative infrared wall inspection*. 10th International Conference on Quantitative Infrared Thermography (2010)

[38] Fokaides, P.A.; Kalogirou, S.A. *Application of infrared thermography for the determination of the overall heat transfer coefficient (U-Value) in building envelopes*. Applied Energy 88 (2011) 4358-4365

[39] Dall'O, G; Sarto, L; Panza, A. *Infrared screening of residential buildings for energy audit purposes: results of a field test*. Energies 6 (2013), 3859-3878

[40] De Freitas, S.S.; de Freitas, V.P.; Barreira, E. *Detection of façade plaster detachments using infrared thermography –A non destructive technique*. Construction and Building Materials 70 (2014) 80-87

[41] Danielski, I; Fröling, M. *Diagnosis of buildings' thermal performance -a quantitative method using thermography under non-steady state heat flow*. 7th Internacional Conference on Sustainability in Energy and Buildings. Energy Procedia (2015) 320-329

[42] American Society for Testing and Materials, 2013. *Standard ASTM C177-13. Standard test method for steady-state heat flux measurements and thermal transmission properties by means of the guarded hot plate apparatus*. 2013

[43] American Society for Testing and Materials, 2011. *Standard ASTM C1363-11. Standard test method for thermal performance of building materials and envelope assemblies by means of a hot box apparatus*

[44] International Organization for Standardization, 1997. *UNE-EN ISO 8990:1997. Thermal insulation. Determination of steady-state thermal transmission properties. Calibrated and guarded hot box*

[45] International Organization for Standardization, 2014. *ISO 9869-1:2014 Thermal insulation. Building elements. In –situ measurement of thermal resistance and thermal transmittance. Part 1: Heat flow meter method*

[46] International Organization for Standardization, 2008. *ISO 18434-1:2008. Condition monitoring and diagnostic of machines. Thermography –Part 1: General procedures*

[47] International Organization for Standardization, 1998. *EN 13187:1998 (ISO 6781:1983 modified). Thermal Performance of Buildings. Qualitative detection of thermal irregularities in building envelopes. Infrared method*

[48] RESNET –Residential Energy Services Network-, 2010. *RESNET Interim Guideline for Thermographic Inspections of Buildings*. Available at: <http://www.resnet.us/standards/RESNET_IR_ interim_guidelines. pdf > (accessed 04.10.16)

[49] International Organization for Standardization, 2018. *ISO 9869-2:2018 Thermal insulation. Building elements. In –situ measurement of thermal resistance and thermal transmittance. Part 2: Infrared method for frame structure dwelling*

[50] Balaras, C.A; Argiriou, A.A. *Infrared thermography for building diagnostics.* Energy and Buildings 34 (2002) 171-183

[51] Datcu, S; Ibos, L; Candau, Y; Mattei, S. *Improvement of building wall surface temperature measurements by infrared thermography.* Infrared Physics & Technology 46 (2005) 451-467

[52] Charlier, L. *Utilisation de la thermographie infrarouge pour la determination des déperditions thermiques d'un bâtiment.* Université de Liége(2007)

[53] Van De Vijver, S; Steeman, M; Van Den Bossche, N; Carbonez, K; Janssens, A. *The influence of environmental parameters on the thermographic analysis of the building envelope.* 12th International Conference on Quantitative Infrared Thermography, Proceedings (2014)

[54] Tejedor, B; Casals, M; Gangolells, M; Roca, X. *Quantitative internal infrared thermography for determining in-situ thermal behaviour of façades.* Energy and Buildings 151 (2017) 187-197

[55] Lucchi, E. *Applications of the infrared thermography in the energy audit of buildings: A review.* Renewable and Sustainable Energy Reviews 82 (2018) 3077-3090

[56] Tejedor, B; Casals, M; Gangolells, M. *Assessing the influence of operating conditions and thermophysical properties on the accuracy of in-situ measured U-values using quantitative internal* infrared *thermography.* Energy and Buildings 171 (2018) 64-75

[57] Vavilov, VP. *A pessimistic view of the energy auditing of building structures with the use of infrared thermography.* Russian Journal of Nondestructive Testing 46 (2010) 906-910

[58] Hoyano, A; Asano, K; Kanamaru, T. *Analysis of the heat flux from the exterior surface of buildings using* time *sequential thermography.* Atmospheric Environment 33 (1999) 3941-3951

[59] Carbonez, K; Van Den Bossche, N; Steeman, M; Van De Vijver, S; Janssens, A. *On the applicability of quantitative infrared thermography on window glazing.* 10th Nordic Symposium on Building Physics, Proceedings (2014) 313-320

[60] Marshall, A; Francou, J; Fitton, R; Swan, R; Owen, W; Benjaber, M. *Variations in the U-value measurements of a whole dwelling using infrared thermography under controlled conditions*. Buildings 8, 46 (2018)

[61] Nardi, I; Lucchi, E; De Rubeis, T; Ambrosini, D. *Quantification of heat energy losses through the building envelope: a state-of-the-art analysis with critical and comprehensive review on infrared thermography*. Buildings and Environment 146 (2018) 190-205

[62] Nardi, I; Sfarra, S; Ambrosini, D. *Quantitative thermography for the estimation of the U-Value: state of art and a case study*. 32nd IUT (Italian Union of Thermo-fluid-dynamics) Heat Transfer Conference, Journal of Physics, Conference Series 547 (2014) 012016

[63] Taylor, T; Counsell, J; Gill, S. *Combining thermography and computer simulation to identify and assess insulation defects in the construction of building façades.* Energy and Buildings 76 (2014) 130-142

[64] Bienvenido-Huertas, D; Rodríguez-Álvaro, R; Moyano, J.J; Rico, F; Marín, D. *Determining the U-value of façades using the thermometric method: potentials and limitations*. Energies 11 (2018) 1-17

[65] Marinetti, S; Cesaratto, P.G. *Emissivity estimation for accurate quantitative thermography*. NDT&E International 51 (2012) 127-134.

[66] Porras-Amores, C; Mazarron, F.R.; Cañas, I. *Using quantitative infrared thermography to determine indoor air temperature*. Energy and Buildings 65 (2013) 292 -298

[67] Ibarra-Castanedo, C; González, D; Klein, M; Pilla, M; Vallerand, S; Maldague, X. *Infrared image processing and data analysis*. Infrared Physics and Technology 46 (2004) 75-83

951 [68] Tsopelas, N; Siakavellas, NJ. *Experimental evaluation of electromagnetic-thermal non-destructive*
952 *inspection by eddy current thermography in square aluminium plates*. NDT & E International 44 (2011)
953 609-620
954
955 [69] Duan, Y; Servais, P; Genest, M; Ibarra-Castanedo, C; Maldague, X. *ThermoPoD: a reliability study*
956 *on active infrared thermography for the inspection of composite materials*. Journal of Mechanical Science
957 and Technology 26 (2012) 1985-1991
958
959 [70] Montanini, R; Quattrocchi, A; Piccolo, S.A. *Active thermography and post-processing image*
960 *enhancement for recovering of abraded and paint-covered alphanumeric identification*. Infrared Physics
961 & Technology 78 (2016) 24-30
962
963 [71] Chrysafi, A.P; Athanasopoulos, N; Siakavellas, N.J. *Damage detection on composite materials with*
964 *active thermography and digital image processing*. International Journal of Thermal Sciences 116 (2017)
965 242-253
966
967 [72] D'Accardi, E; Palumbo, E; Tamborrino, R; Galietti, U. *Quantitative analysis of thermographic data*
968 *through different algorithms.* Procedia Structural Integrity 8 (2018) 354-367
969
970 [73] Diagnostic Engineering Solutions S.R.L, 2017. IRTA Software
971
972 [74] MathWorks, 2016. Programming Environmental Toolbox, MATLAB Software
973
974 [75] MathWorks, 2018. System Identification Tool, MATLAB Software
975
976 [76] Nardi, I; Ambrosini, D; de Rubeis, T; Sfarra, S; Perilli, S; Pasqualoni, G. *A comparison between*
977 *thermographic and flow-meter methods for the evaluation of thermal transmittance of different wall*
978 *constructions*. Journal of Physics, Conference Series 655 (2015) 012007"
979

980 [77] O'Grady, A.M.; Lechowska, A.A.; Harte, A.M. *Infrared thermography technique as an in-situ*
981 *method of assessing heat loss through thermal bridging*. Energy and Buildings 135 (2017) 20 - 32"
982
983 [78] Spain, 1979. *Royal Decree 2429/1979 approving the Basic Building Norm on Thermal Conditions*
984 *in Buildings NBE-CT-79*. Available at: < https://www.boe.es/boe/dias/1979/10/22/pdfs/A24524-
985 24550.pdf> (accessed 04.10.16)
986
987 [79] Spain, 2006. *Royal Decree 314/2006 approving the Spanish Technical Building Code CTE-DB-HE1*.
988 Available at: < http://www.boe.es/boe/dias/2006/03/28/pdfs/A11816-11831.pdf > (accessed 04.10.16)
989
990 [80] International Organization for Standardization, 2012. *UNE EN ISO 6946:2012 Building components*
991 *and building elements. Thermal resistance and thermal transmittance. Calculation method*
992
993 [81] International Organization for Standardization, 2011. *UNE EN ISO 13786:2011 Thermal*
994 *performance of building components –Dynamic thermal characteristics –Calculation methods*
995
996 [82] International Organization for Standardization, 2012. *UNE EN ISO 10456:2012 Building materials*
997 *and products –Hygrothermal properties –Tabulated design values and procedures for determining*
998 *declared and design thermal values*, 2012
999
1000 [83] FLIR Systems, 2015. FLIR TOOLS+ Software
1001
1002 [84] Yaffee, R.A.; McGee, M. *Introduction to time series analysis and forecasting: with applications of*
1003 *SAS and SPSS*. Academic Press (2000)
1004
1005 [85] Mahan, M.Y; Chron, C.R; Georgopoulos, A.P. *White noise test: detecting autocorrelation and*
1006 *nonstationarities in long time series after ARIMA modelling*. Proceedings of the 14th Python in Science
1007 Conference (SCYPY 2015)
1008

1009 [86] Andersen, K.K.; Madsen, H; Hansen, L.H. *Modelling the heat dynamics of a building using*
1010 *stochastic differential equations*. Energy and Buildings 31 (2000) 13-24
1011
1012 [87] Bacher, P; Madsen, H. *Identifying suitable models for the heat dynamics of buildings*. Energy and
1013 Buildings 43 (2011) 1511-1522
1014
1015 [88] Macarulla, M; Casals, M; Carnevali, M; Forcada, N; Gangolells, M. *Modelling indoor air carbon*
1016 *dioxide concentration using grey-box models*. Building and Environment 117 (2017) 146-153
1017
1018 [89] Macarulla, M; Casals, M; Forcada, N; Gangolells, M; Giretti, A. *Estimation of a room ventilation air*
1019 *change rate* using *a stochastic grey-box modelling approach.* Measurement 124 (2018) 539-548
1020
1021 [90] Meko, D. *Notes on Autocorrelation, Notes 3, GEOS 585A, from the course Applied Time Series*
1022 *Analysis*. University of Arizona, 2010. Available at: <http://www.ltrr.arizona.edu/~dmeko/
1023 geos585a.html#chandout> (accessed 20.02.18)
1024
1025 [91] Rust, B.W; O'Leary, D.P. *Residual periodograms for choosing regularization parameters for ill-*
1026 *posed* problems. IOP Science. Inverse Problems 24 (2008)
1027
1028 [92] Fuller, W.A. *Introduction to statistical time series*. John Wiley and Sons. pp. 363-366. New York
1029 1996
1030
1031 [93] Box, G.; Jenkins, G. *Time series analysis: forecasting and control*. Holden Day, 2nd Edition (1976)
1032
1033 [94] Anderson, O.D. *The Box-Jenkins approach to time series analysis.* RAIRO 11 (1977) 3-29
1034
1035 [95] Huitema, B.E.; McKean, J.W. *Autocorrelation estimation and inference with small samples*.
1036 Physicological Bulletin 110 (1991) 291-304
1037

[96] De Carlo, L.T.; Tryon, W.W. *Estimating and testing autocorrelation with small samples: a comparison of the C-Statistic to a modified estimator*. Behav. Res. Ther. 31 (1993) 781-788

[97] Lúnden, O; Bäckström, M. *Stirrer efficiency in FOA reverberation chambers. Evaluation of correlation coefficients and chi-squared tests*. Proc. IEEE Int.Symp.Electromagn.Compat. 1 (2000) 11-16

[98] Plane, D.R.; Gordon, K.R. *A simple proof of no applicability of the central limit theorem to finite populations.* The American statistician 36 (1982) 175-176

[99] Chang, H-J; Chen, P-Y. *On sample size in using central limit theorem for gamma distribution.* Information and Management Sciences 19 (2008) 153-174

[100] Wiener, N. *Extrapolation, Interpolation and Smoothing of Stationary Time Series*. John Wiley & Sons. New York, 2013 (Reprint of 1949 Edition). ISBN 1-614-27517-3

[101] Brown, R.G.; Hwang, P. *Introduction to Random Signals and Applied Kalman Filtering*. John Wiley & Sons. New York, 1996. ISBN 0-471-12839-2

[102] Beck, J.V.; Blackwell, A; Haji-Sheich. *Comparison of some inverse heat conduction methods using experimental data*. International Journal of Heat Mass Transfer 39 (1996) 3649-3657

[103] Ilyinsky, A.L.; Rainieri, S; Farina, A; Pagliarini, G. *New Experimental Tecnhique for Enhancement of Spatial Resolution in Heat Transfer Measurements*. Proceedings 4th World Conference on Experimental Heat Transfer, Fluid Mechanics and Thermodynamics, vol.1 (1997) 93-100

[104] Le Niliot, C; Gallet, P. *Infrared thermography applied to the resolution on inverse heat conduction problems: recovery of heat line sources and boundary conditions*. Revue Générale de Thermique 37 (1998) 629-643

[105] Rainieri, S; Pagliarini, G. *Performance Analysis of a FPA IR Camera for Surface Heat Flux Restoration*. Proceedings of the 8th International Symposium on Flow Visualization Sorrento (1998) 1-4

[106] Rainieri, S; Pagliarini, G. *Data filtering applied to infrared thermographic measurements intended for the estimation of local heat transfer coefficient*. Experimental Thermal and Fluid Science 26 (2002) 109-114

[107] MathWorks, 1998. Signal Processing Toolbox, MATLAB Software

[108] MathWorks, 1998. Image Processing Toolbox, MATLAB Software

[109] Jiménez, M.J; Madsen, H; Andersen, K.K. *Identification of the main thermal characteristics of building components using MATLAB*. Building and Environment 43 (2008) 170-180

[110] MathWorks, 2006. IDENT Toolbox, MATLAB Software

[111] Rachad, S; Nsiri, B; Bensassi, B. *System Identifiaction of Inventory System using ARX and ARMAX models*. International Journal of Control and Automation 8 (2015) 283 - 294

[112] Touloukian, Y.S.; Liley, P.E.; Saxena, S.C. *Thermophysical Properties of Matter. Volume 3. Thermal Conductivity*. IFI/Plenum. New York, 1970. ISBN 978-0-306-67020-6

[113] Touloukian, Y.S.; Saxena, S.C.; Hestermans, P. *Thermophysical Properties of Matter. Volume 11. Viscosity*. IFI/Plenum. New York, 1970. ISBN 978-1-475-71630-6

[114] Keenan, J.H; Chao, J; Kaye, J. *Gas Tables –International Version*. John Wiley & Sons. New York, 1983. ISBN 0-471-08874-9

[115] Dixon, C. *The Shock Absorber Handbook. Appendix B. Properties of air*. Second Edition. John Wiley & Sons. New York, 2007. ISBN 978-0-470-51020-9

[116] Serth, R.W. *Process heat transfer: Principles and Applications. Chapter 2: Convective heat transfer*. Elsevier, 2007, p.43-84, ISBN 978-0-12-373588-1

[117] F-Chart Software, 2016. EES Software

[118] American Society for Testing and Materials, 2013. *Standard ASTM C1555-95 (2013). Standard practice for determining thermal resistance of building envelope components from the in-situ data*

[119] Gaspar, K; Casals, M; Gangolells, M. *In-situ measurement of façades with a low U-value: Avoiding deviations*. Energy and Buildings 170 (2018) 61-73

- A gap in standardization of quantitative IRT was detected
- Research was undertaken in six real built environments
- Measured U-values might be assumed as a constant signal plus white noise
- 30 minutes could be enough to obtain reliable results of in-situ measured U-values
- A routine for stopping quantitative IRT tests in real time is proposed